

## Chapter 8

# Wavelet Transform

The *wavelet transform* was introduced at the beginning of the 1980s by Morlet *et al.*, who used it to evaluate seismic data [105],[106]. Since then, various types of wavelet transforms have been developed, and many other applications have been found. The continuous-time wavelet transform, also called the *integral wavelet transform* (IWT), finds most of its applications in data analysis, where it yields an affine invariant time-frequency representation. The most famous version, however, is the discrete wavelet transform (DWT). This transform has excellent signal compaction properties for many classes of real-world signals while being computationally very efficient. Therefore, it has been applied to almost all technical fields including image compression, denoising, numerical integration, and pattern recognition.

### 8.1 The Continuous-Time Wavelet Transform

The wavelet transform  $\mathcal{W}_x(b, a)$  of a continuous-time signal  $x(t)$  is defined as

$$\mathcal{W}_x(b, a) = |a|^{-\frac{1}{2}} \int_{-\infty}^{\infty} x(t) \psi^* \left( \frac{t-b}{a} \right) dt. \quad (8.1)$$

Thus, the wavelet transform is computed as the inner product of  $x(t)$  and translated and scaled versions of a single function  $\psi(t)$ , the so-called *wavelet*.

If we consider  $\psi(t)$  to be a bandpass impulse response, then the wavelet analysis can be understood as a bandpass analysis. By varying the scaling

parameter  $a$  the center frequency and the bandwidth of the bandpass are influenced. The variation of  $b$  simply means a translation in time, so that for a fixed  $a$  the transform (8.1) can be seen as a convolution of  $x(t)$  with the time-reversed and scaled wavelet:

$$\mathcal{W}_x(t, a) = |a|^{-\frac{1}{2}} x(t) * \psi_a(t), \quad \psi_a(t) = \psi^* \left( \frac{-t}{a} \right).$$

The prefactor  $|a|^{-1/2}$  is introduced in order to ensure that all scaled functions  $|a|^{-1/2} \psi^*(t/a)$  with  $a \in \mathbb{R}$  have the same energy.

Since the analysis function  $\psi(t)$  is scaled and not modulated like the kernel of the STFT, a wavelet analysis is often called a *time-scale analysis* rather than a time-frequency analysis. However, both are naturally related to each other by the bandpass interpretation. Figure 8.1 shows examples of the kernels of the STFT and the wavelet transform. As we can see, a variation of the time delay  $b$  and/or of the scaling parameter  $a$  has no effect on the form of the transform kernel of the wavelet transform. However, the time and frequency resolution of the wavelet transform depends on  $a$ . For high analysis frequencies (small  $a$ ) we have good time localization but poor frequency resolution. On the other hand, for low analysis frequencies, we have good frequency but poor time resolution. While the STFT is a constant bandwidth analysis, the wavelet analysis can be understood as a constant- $Q$  or octave analysis.

When using a transform in order to get better insight into the properties of a signal, it should be ensured that the signal can be perfectly reconstructed from its representation. Otherwise the representation may be completely or partly meaningless. For the wavelet transform the condition that must be met in order to ensure perfect reconstruction is

$$C_\psi = \int_{-\infty}^{\infty} \frac{|\Psi(\omega)|^2}{|\omega|} d\omega < \infty, \quad (8.2)$$

where  $\Psi(\omega)$  denotes the Fourier transform of the wavelet. This condition is known as the *admissibility condition* for the wavelet  $\psi(t)$ . The proof of (8.2) will be given in Section 8.3.

Obviously, in order to satisfy (8.2) the wavelet must satisfy

$$\Psi(0) = \int_{-\infty}^{\infty} \psi(t) dt = 0. \quad (8.3)$$

Moreover,  $|\Psi(\omega)|$  must decrease rapidly for  $|\omega| \rightarrow 0$  and for  $|\omega| \rightarrow \infty$ . That is,  $\psi(t)$  must be a bandpass impulse response. Since a bandpass impulse response looks like a small wave, the transform is named wavelet transform.

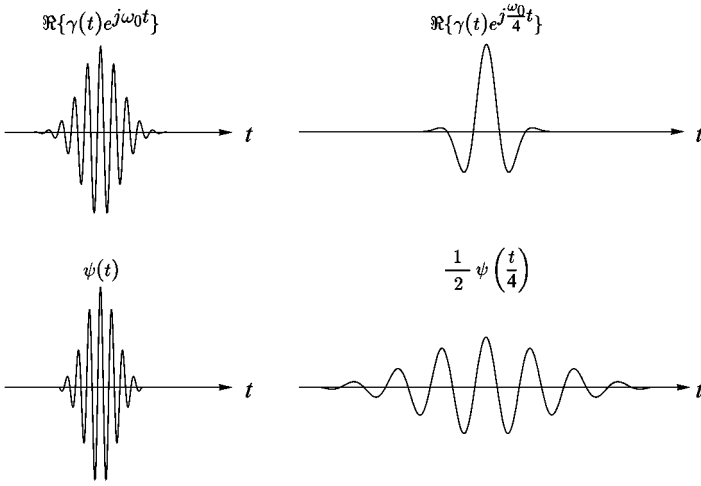


**Figure 8.1.** Comparison of the analysis kernels of the short-time Fourier transform (top, the real part is shown) and the wavelet transform (bottom, real wavelet) for high and low analysis frequencies.

**Calculation of the Wavelet Transform from the Spectrum  $X(\omega)$ .**

Using the abbreviation

$$\psi_{b,a}(t) = |a|^{-\frac{1}{2}} \psi\left(\frac{t-b}{a}\right) \tag{8.4}$$

the integral wavelet transform introduced by equation (8.1) can also be written as

$$\mathcal{W}_x(b, a) = \langle x, \psi_{b,a} \rangle. \tag{8.5}$$

With the correspondences  $X(\omega) \longleftrightarrow x(t)$  and  $\Psi(\omega) \longleftrightarrow \psi(t)$ , and the time and frequency shift properties of the Fourier transform, we obtain

$$\begin{aligned} \Psi_{b,a}(\omega) &= |a|^{\frac{1}{2}} e^{-j\omega b} \Psi(a\omega) \\ &\updownarrow \\ \psi_{b,a}(t) &= |a|^{-\frac{1}{2}} \psi\left(\frac{t-b}{a}\right). \end{aligned} \tag{8.6}$$

By making use of Parseval's relation we finally get

$$\begin{aligned} \mathcal{W}_x(b, a) &= \frac{1}{2\pi} \langle X, \Psi_{b,a} \rangle \\ &= |a|^{\frac{1}{2}} \frac{1}{2\pi} \int_{-\infty}^{\infty} X(\omega) \Psi^*(a\omega) e^{j\omega b} d\omega. \end{aligned} \tag{8.7}$$

Equation (8.7) states that the wavelet transform can also be calculated by means of an inverse Fourier transform from the windowed spectrum  $X(\omega) \Psi^*(a\omega)$ .

**Time-Frequency Resolution.** In order to describe the time-frequency resolution of the wavelet transform we consider the time-frequency window associated with the wavelet. The center  $(t_0, \omega_0)$  and the radii  $\Delta_t$  and  $\Delta_\omega$  of the window are calculated according to (7.8) and (7.11). This gives

$$t_0 = \int_{-\infty}^{\infty} t \cdot \frac{|\psi(t)|^2}{\|\psi\|^2} dt, \tag{8.8}$$

$$\omega_0 = \int_{-\infty}^{\infty} \omega \cdot \frac{|\Psi(\omega)|^2}{\|\Psi\|^2} d\omega \tag{8.9}$$

and

$$\Delta_t = \left( \int_{-\infty}^{\infty} (t - t_0)^2 \cdot \frac{|\psi(t)|^2}{\|\psi\|^2} dt \right)^{\frac{1}{2}}, \tag{8.10}$$

$$\Delta_\omega = \left( \int_{-\infty}^{\infty} (\omega - \omega_0)^2 \cdot \frac{|\Psi(\omega)|^2}{\|\Psi\|^2} d\omega \right)^{\frac{1}{2}}. \tag{8.11}$$

For the center and the radii of the scaled function  $\psi(\frac{t}{a}) \longleftrightarrow |a|\Psi(a\omega)$  we have  $\{a \cdot t_0, \frac{1}{a}\omega_0\}$  and  $\{a \cdot \Delta_t, \frac{1}{a}\Delta_\omega\}$ , respectively. This means that the wavelet transform  $\mathcal{W}_x(b, a)$  provides information on a signal  $x(t)$  and its spectrum  $X(\omega)$  in the time-frequency window

$$[b + a \cdot t_0 - a \cdot \Delta_t, b + a \cdot t_0 + a \cdot \Delta_t] \times \left[ \frac{\omega_0}{a} - \frac{\Delta_\omega}{a}, \frac{\omega_0}{a} + \frac{\Delta_\omega}{a} \right]. \tag{8.12}$$

The area  $4\Delta_t\Delta_\omega$  is independent of the parameters  $a$  and  $b$ ; it is determined only by the used wavelet  $\psi(t)$ . The time window narrows when  $a$  becomes small, and it widens when  $a$  becomes large. On the other hand, the frequency window becomes wide when  $a$  becomes small, and it becomes narrow when  $a$  becomes large. As mentioned earlier, a short analysis window leads to good time resolution on the one hand, but on the other to poor frequency resolution. Accordingly, a long analysis window yields good frequency resolution but poor time resolution. Figure 8.2 illustrates the different resolutions of the short-time Fourier transform and the wavelet transform.

**Affine Invariance.** Equation (8.1) shows that if the signal is scaled ( $x(t) \rightarrow x(t/c)$ ), the wavelet representation  $\mathcal{W}_x(b, a)$  is scaled as well; except this,  $\mathcal{W}_x(b, a)$  undergoes no other modification. For this reason we also speak of an

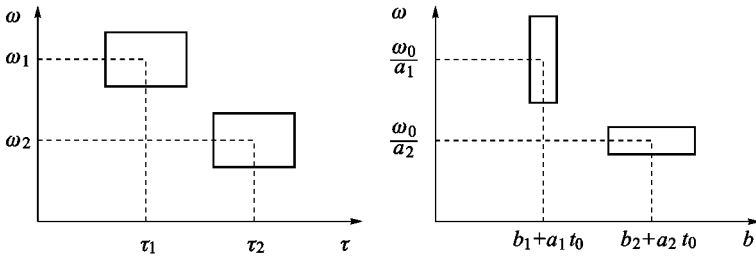


**Figure 8.2.** Resolution of the short-time Fourier transform (left) and the wavelet transform (right).

*affine invariant transform.* Furthermore, the wavelet transform is *translation invariant*, i.e. a shift of the signal ( $x(t) \rightarrow x(t - t_0)$ ) leads to a shift of the wavelet representation  $\mathcal{W}_x(b, a)$  by  $t_0$ , but  $\mathcal{W}_x(b, a)$  undergoes no other modification.

## 8.2 Wavelets for Time-Scale Analysis

In time-scale signal analysis one aims at inferring certain signal properties from the wavelet transform in a convenient way. *Analytic wavelets* are especially suitable for this purpose. Like an *analytic signal*, they contain only positive frequencies. In other words, for the Fourier transform of an analytic wavelet  $\psi_{b,a}(t)$  the following holds:

$$\Psi_{b,a}(\omega) = 0 \quad \text{for} \quad \omega \leq 0. \tag{8.13}$$

Analytic wavelets have a certain property, which will be discussed briefly below. For this consider the real signal  $x(t) = \cos(\omega_0 t)$ . The spectrum is

$$X(\omega) = \pi [\delta(\omega - \omega_0) + \delta(\omega + \omega_0)] \longleftrightarrow x(t) = \cos(\omega_0 t). \tag{8.14}$$

Substituting  $X(\omega)$  according to (8.14) into (8.7) yields

$$\begin{aligned} \mathcal{W}_x(b, a) &= \frac{1}{2} |a|^{\frac{1}{2}} \int_{-\infty}^{\infty} (\delta(\omega - \omega_0) + \delta(\omega + \omega_0)) \Psi^*(a\omega) e^{j\omega b} d\omega \\ &= \frac{1}{2} |a|^{\frac{1}{2}} \left[ \Psi^*(a\omega_0) e^{j\omega_0 b} + \Psi^*(-a\omega_0) e^{-j\omega_0 b} \right]. \end{aligned} \tag{8.15}$$

Hence, for an analytic wavelet:

$$\mathcal{W}_x(b, a) = \frac{1}{2} |a|^{\frac{1}{2}} \Psi^*(a\omega_0) e^{j\omega_0 b}. \tag{8.16}$$

Since only the argument of the complex exponential in (8.16) depends on  $b$ , the frequency of  $x(t)$  can be inferred from the phase of  $\mathcal{W}_x(b, a)$ . For this, any horizontal line in the time-frequency plane can be considered. The magnitude of  $\mathcal{W}_x(b, a)$  is independent of  $b$ , so that the amplitude of  $x(t)$  can be seen independent of time. This means that the magnitude of  $\mathcal{W}_x(b, a)$  directly shows the time-frequency distribution of signal energy.

**The Scalogram.** A *scalogram* is the squared magnitude of the wavelet transform:

$$|\mathcal{W}_x(b, a)|^2 = \left| |a|^{-\frac{1}{2}} \int_{-\infty}^{\infty} x(t) \psi^* \left( \frac{t-b}{a} \right) dt \right|^2. \quad (8.17)$$

Scalograms, like spectrograms, can be represented as images in which intensity is expressed by different shades of gray. Figure 8.3 depicts scalograms for  $x(t) = \delta(t)$ . We see that here analytic wavelets should be chosen in order to visualize the distribution of the signal energy in relation to time and frequency (and scaling, respectively).

**The Morlet Wavelet.** The complex wavelet most frequently used in signal analysis is the Morlet wavelet, a modulated Gaussian function:

$$\psi(t) = e^{j\omega_0 t} e^{-\beta^2 t^2 / 2}. \quad (8.18)$$

Note that the Morlet wavelet satisfies the admissibility condition (8.2) only approximately. However, by choosing proper parameters  $\omega_0$  and  $\beta$  in (8.18) one can make the wavelet at least “practically” admissible. In order to show this, let us consider the Fourier transform of the wavelet, which, for  $\omega = 0$ , does not vanish exactly:

$$\Psi(\omega) = \frac{1}{\beta} e^{-(\omega - \omega_0)^2 / (2\beta^2)} > 0 \quad \forall \omega. \quad (8.19)$$

By choosing

$$\omega_0 \geq 2\pi\beta \quad (8.20)$$

we get  $\Psi(\omega) \leq 2.7 \times 10^{-9}$  for  $\omega \leq 0$ , which is sufficient for most applications [132]. Often  $\omega_0 \geq 5\beta$  is taken to be sufficient [65], which leads to  $\Psi(\omega) \leq 10^{-5}$ ,  $\omega \leq 0$ .

**Example.** The example considered below is supposed to give a visual impression of a wavelet analysis and illustrates the difference from a short-time Fourier analysis. The chosen test signal is a discrete-time signal; it contains

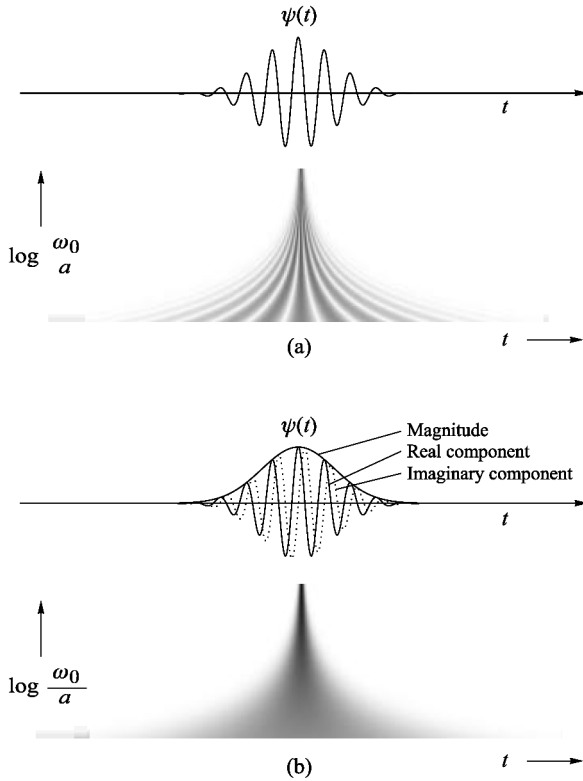


**Figure 8.3.** Scalogram of a delta impulse ( $\mathcal{W}_\delta(b, a) = |\psi(b/a)|^2$ ); (a) real wavelet; (b) analytic wavelet.

two periodic parts and two impulses.<sup>1</sup> An almost analytic, sampled Morlet wavelet is used. The signal is depicted in Figure 8.4(a). Figures 8.4(b) and 8.4(c) show two corresponding spectrograms (short-time Fourier transforms) with Gaussian analysis windows. We see that for a very short analysis window the discrimination of the two periodic components is impossible whereas the impulses are quite visible. A long window facilitates good discrimination of the periodic component, but the localization of the impulses is poor. This is not the case in the wavelet analysis represented in Figure 8.4(d). Both the periodic components and the impulses are clearly visible. Another property of the wavelet analysis, which is well illustrated in Figure 8.4(d), is that it clearly indicates non-stationarities of the signal.

<sup>1</sup>In Section 8.8 the question of how the wavelet transform of a discrete-time signal can be calculated will be examined in more detail.

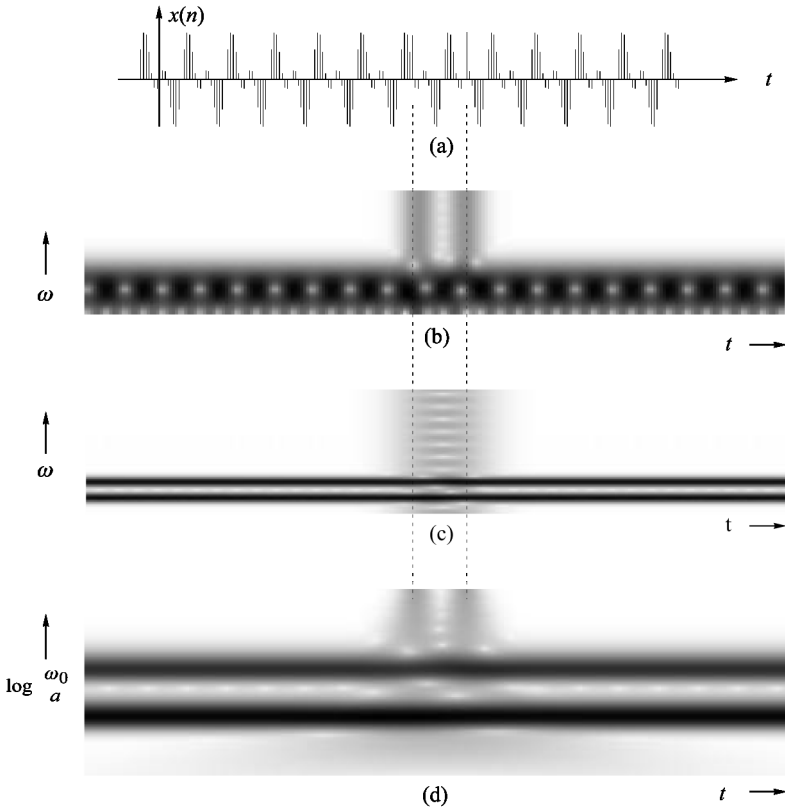


**Figure 8.4.** Examples of short-time Fourier and wavelet analyses; (a) test signal; (b) spectrogram (short window); (c) spectrogram (long window); (d) scalogram.

### 8.3 Integral and Semi-Discrete Reconstruction

In this section, two variants of continuous wavelet transforms will be considered; they only differ in the way reconstruction is handled. Specifically, we will look at integral reconstruction from the entire time-frequency plane and at a semi-discrete reconstruction.

#### 8.3.1 Integral Reconstruction

As will be shown, the inner product of two signals  $x(t)$  and  $y(t)$  is related to the inner product of their wavelet transforms as

$$\langle \mathbf{x}, \mathbf{y} \rangle = \frac{1}{C_\psi} \int_{-\infty}^{\infty} \int_{-\infty}^{\infty} \mathcal{W}_x(b, a) \mathcal{W}_y^*(b, a) \frac{da db}{a^2} \tag{8.21}$$

with  $C_\psi$  as in (8.2).

Given the inner product (8.21), we obtain a synthesis equation by choosing

$$y_t(t') = \delta(t' - t), \quad (8.22)$$

because then the following relationship holds:

$$\langle \mathbf{x}, \mathbf{y}_t \rangle = \int_{-\infty}^{\infty} f(t') \delta(t' - t) dt' = x(t). \quad (8.23)$$

Substituting (8.22) into (8.21) gives

$$\langle \mathbf{x}, \mathbf{y}_t \rangle = \frac{1}{C_\psi} \int_{-\infty}^{\infty} \int_{-\infty}^{\infty} \mathcal{W}_x(b, a) |a|^{-\frac{1}{2}} \int_{-\infty}^{\infty} \delta(t' - t) \psi\left(\frac{t' - b}{a}\right) dt' \frac{da db}{a^2}.$$

From this we obtain the reconstruction formula

$$x(t) = \frac{1}{C_\psi} \int_{-\infty}^{\infty} \int_{-\infty}^{\infty} \mathcal{W}_x(b, a) |a|^{-\frac{1}{2}} \psi\left(\frac{t - b}{a}\right) \frac{da db}{a^2}. \quad (8.24)$$

*Proof of (8.2) and (8.21).* With

$$P_a(\omega) = X(\omega) \Psi^*(\omega a) \quad (8.25)$$

equation (8.7) can be written as

$$\mathcal{W}_x(b, a) = |a|^{\frac{1}{2}} \frac{1}{2\pi} \int_{-\infty}^{\infty} P_a(\omega) e^{j\omega b} d\omega. \quad (8.26)$$

Using the correspondence  $P_a(\omega) \longleftrightarrow p_a(b)$  we obtain

$$\mathcal{W}_x(b, a) = |a|^{\frac{1}{2}} p_a(b). \quad (8.27)$$

Similarly, for the wavelet transform of  $y(t)$  we get

$$Q_a(\omega) = Y(\omega) \Psi^*(\omega a) \longleftrightarrow q_a(b), \quad (8.28)$$

which means that

$$\mathcal{W}_y(b, a) = |a|^{\frac{1}{2}} q_a(b). \quad (8.29)$$

Substituting (8.27) and (8.28) into the right term of (8.21) and rewriting the obtained expression by applying Parseval's relation yields

$$\begin{aligned}
 \int_{-\infty}^{\infty} \int_{-\infty}^{\infty} \mathcal{W}_x(b, a) \mathcal{W}_y^*(b, a) \frac{da db}{a^2} &= \int_{-\infty}^{\infty} \frac{1}{|a|} \int_{-\infty}^{\infty} p_a(b) q_a^*(b) db da \\
 &= \int_{-\infty}^{\infty} \frac{1}{|a|} \langle \mathbf{p}_a, \mathbf{q}_a \rangle da \\
 &= \int_{-\infty}^{\infty} \frac{1}{|a|} \frac{1}{2\pi} \langle \mathbf{P}_a, \mathbf{Q}_a \rangle da \\
 &= \frac{1}{2\pi} \int_{-\infty}^{\infty} X(\nu) Y^*(\nu) \int_{-\infty}^{\infty} \frac{|\Psi(\nu a)|^2}{|a|} da d\nu.
 \end{aligned} \tag{8.30}$$

By substituting  $\omega = \nu a$  we can show that the inner integral in the last line of (8.30) is a constant, which only depends on  $\psi(t)$ :

$$C_\psi = \int_{-\infty}^{\infty} \frac{|\Psi(\nu a)|^2}{|a|} da = \int_{-\infty}^{\infty} \frac{|\Psi(\omega)|^2}{|\omega|} d\omega. \tag{8.31}$$

Hence (8.30) is

$$\begin{aligned}
 \int_{-\infty}^{\infty} \int_{-\infty}^{\infty} \mathcal{W}_x(b, a) \mathcal{W}_y^*(b, a) \frac{da db}{a^2} &= C_\psi \frac{1}{2\pi} \int_{-\infty}^{\infty} X(\nu) Y^*(\nu) d\nu \\
 &= C_\psi \int_{-\infty}^{\infty} x(\tau) y^*(\tau) d\tau.
 \end{aligned} \tag{8.32}$$

This completes the proof of (8.2) and (8.21).  $\square$

### 8.3.2 Semi-Discrete Dyadic Wavelets

We speak of semi-discrete dyadic wavelets if every signal  $x(t) \in L_2(\mathbb{R})$  can be reconstructed from semi-discrete values  $\mathcal{W}_x(b, a_m)$ , where  $a_m, m \in \mathbb{Z}$  are dyadically arranged:

$$a_m = 2^m. \tag{8.33}$$

That is, the wavelet transform is calculated solely along the lines  $\mathcal{W}_x(b, 2^m)$ :

$$\mathcal{W}_x(b, 2^m) = 2^{-\frac{m}{2}} \int_{-\infty}^{\infty} x(t) \psi^*(2^{-m}(t - b)) dt. \tag{8.34}$$

The center frequencies of the scaled wavelets are

$$\omega_m = \frac{\omega_0}{a_m} = 2^{-m} \omega_0, \quad m \in \mathbb{Z}, \quad (8.35)$$

with  $\omega_0$  according to (8.9). The radii of the frequency windows are

$$\frac{\Delta_\omega}{a_m} = 2^{-m} \Delta_\omega, \quad m \in \mathbb{Z}. \quad (8.36)$$

In order to ensure that neighboring frequency windows

$$\left[ \frac{\omega_0 - \Delta_\omega}{a_m}, \frac{\omega_0 + \Delta_\omega}{a_m} \right]$$

and

$$\left[ \frac{\omega_0 - \Delta_\omega}{a_{m+1}}, \frac{\omega_0 + \Delta_\omega}{a_{m+1}} \right]$$

do adjoin, we assume

$$\omega_0 = 3 \Delta_\omega. \quad (8.37)$$

This condition can easily be satisfied, because by modulating a given wavelet  $\psi_o(t)$  the center frequency can be varied freely. From (8.33), (8.35) and (8.37) we get for the center frequencies of the scaled wavelets:

$$\omega_m = 3 \cdot 2^{-m} \Delta_\omega, \quad m \in \mathbb{Z}. \quad (8.38)$$

**Synthesis.** Consider the signal analysis and synthesis shown in Figure 8.5. Mathematically, we have the following synthesis approach using a dual (also dyadic) wavelet  $\tilde{\psi}(t)$ :

$$x(t) = \sum_{m=-\infty}^{\infty} 2^{-\frac{3}{2}m} \int_{-\infty}^{\infty} \mathcal{W}_x(b, 2^m) \tilde{\psi}(2^{-m}(t-b)) db. \quad (8.39)$$

In order to express the required dual wavelet  $\tilde{\psi}(t)$  by  $\psi(t)$ , (8.39) is rearranged

as

$$\begin{aligned}
 x(t) &= \sum_{m=-\infty}^{\infty} 2^{-\frac{3}{2}m} \int_{-\infty}^{\infty} \mathcal{W}_x(b, 2^m) \tilde{\psi}(2^{-m}(t-b)) db \\
 &= \sum_{m=-\infty}^{\infty} 2^{-\frac{3}{2}m} \langle \mathcal{W}_x(\cdot, 2^m), \tilde{\psi}^*(2^{-m}(t-\cdot)) \rangle \\
 &= \sum_{m=-\infty}^{\infty} 2^{-\frac{3}{2}m} \frac{1}{2\pi} \langle \mathcal{F} \{ \mathcal{W}_x(\cdot, 2^m) \}, \mathcal{F} \{ \tilde{\psi}^*(2^{-m}(t-\cdot)) \} \rangle \\
 &= \sum_{m=-\infty}^{\infty} 2^{-\frac{3}{2}m} \frac{1}{2\pi} \int_{-\infty}^{\infty} [X(\omega) 2^{\frac{m}{2}} \Psi^*(2^m\omega)] [2^m \tilde{\Psi}(2^m\omega) e^{j\omega t}] d\omega \\
 &= \frac{1}{2\pi} \int_{-\infty}^{\infty} X(\omega) \left[ \sum_{m=-\infty}^{\infty} \Psi^*(2^m\omega) \tilde{\Psi}(2^m\omega) \right] e^{j\omega t} d\omega.
 \end{aligned} \tag{8.40}$$

For the sum in the last row of (8.40)

$$\sum_{m=-\infty}^{\infty} \Psi^*(2^m\omega) \tilde{\Psi}(2^m\omega) = 1 \tag{8.41}$$

must hold in order to allow reconstruction. Hence,  $\tilde{\psi}(t)$  can be computed from  $\psi(t)$  as

$$\tilde{\Psi}(\omega) = \frac{\Psi(\omega)}{\sum_{m=-\infty}^{\infty} |\Psi(2^m\omega)|^2}. \tag{8.42}$$

If two positive constants  $A$  and  $B$  with  $0 < A \leq B < \infty$  exist such that

$$A \leq \sum_{m=-\infty}^{\infty} |\Psi(2^m\omega)|^2 \leq B \tag{8.43}$$

we achieve stability. Therefore, (8.43) is referred to as a *stability condition*. A wavelet  $\psi(t)$  which satisfies (8.43) is called a dyadic wavelet. Note that because of (8.42), for the dual dyadic wavelet, we have:

$$\frac{1}{B} \leq \sum_{m=-\infty}^{\infty} |\tilde{\Psi}(2^m\omega)|^2 \leq \frac{1}{A}. \tag{8.44}$$

Thus, for  $\tilde{\Psi}(\omega)$  according to (8.42) we have stability, provided that (8.43) is satisfied. Note that the dual wavelet is not necessarily unique [25]. One may find other duals that also satisfy the stability condition.

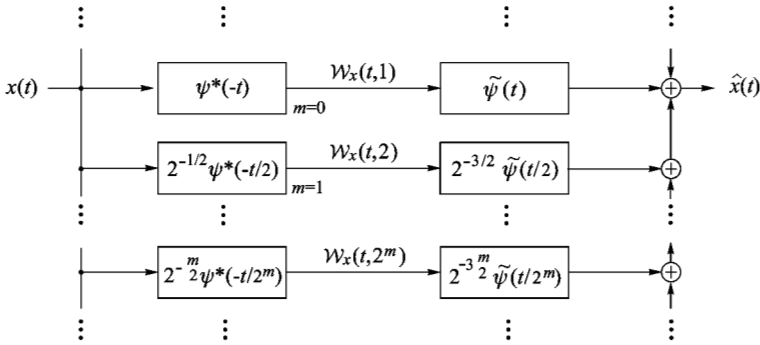


**Figure 8.5.** Octave-band analysis and synthesis filter bank.

Finally it will be shown that if condition (8.43) holds the admissibility condition (8.2) is also satisfied. Dividing (8.43) by  $\omega$  and integrating the obtained expression over the interval  $(1, 2)$  yields:

$$A \int_1^2 \frac{d\omega}{\omega} \leq \sum_{m=-\infty}^{\infty} \int_1^2 \frac{|\Psi(2^m \omega)|^2}{\omega} d\omega \leq B \int_1^2 \frac{d\omega}{\omega}. \quad (8.45)$$

With

$$\int_1^2 \frac{|\Psi(2^m \omega)|^2}{\omega} d\omega = \int_{2^m}^{2^{m+1}} \frac{|\Psi(\nu)|^2}{\nu} d\nu \quad (8.46)$$

we obtain the following result for the center term in (8.45):

$$\sum_{m=-\infty}^{\infty} \int_1^2 \frac{|\Psi(2^m \omega)|^2}{\omega} d\omega = \int_0^{\infty} \frac{|\Psi(\omega)|^2}{\omega} d\omega. \quad (8.47)$$

Thus

$$A \ln 2 \leq \int_0^{\infty} \frac{|\Psi(\omega)|^2}{\omega} d\omega \leq B \ln 2. \quad (8.48)$$

Dividing (8.43) by  $-\omega$  and integrating over  $(-1, -2)$  gives

$$A \ln 2 \leq \int_0^{\infty} \frac{|\Psi(-\omega)|^2}{\omega} d\omega \leq B \ln 2. \quad (8.49)$$

Thus the admissibility condition (8.2) is satisfied in any case, and reconstruction according to (8.24) is also possible.

## 8.4 Wavelet Series

### 8.4.1 Dyadic Sampling

In this section, we consider the reconstruction from discrete values of the wavelet transform. The following dyadically arranged sampling points are used:

$$a_m = 2^m, \quad b_{mn} = a_m n T = 2^m n T, \quad (8.50)$$

This yields the values  $\mathcal{W}_x(b_{mn}, a_m) = \mathcal{W}_x(2^m n T, 2^m)$ . Figure 8.6 shows the sampling grid.

Using the abbreviation

$$\begin{aligned} \psi_{mn}(t) &= |a_m|^{-\frac{1}{2}} \cdot \psi\left(\frac{t - b_{mn}}{a_m}\right) \\ &= 2^{-\frac{m}{2}} \cdot \psi(2^{-m}t - nT), \end{aligned} \quad (8.51)$$

we may write the wavelet analysis as

$$\mathcal{W}_x(b_{mn}, a_m) = \mathcal{W}_x(2^m n T, 2^m) = \langle \mathbf{x}, \psi_{mn} \rangle. \quad (8.52)$$

The values  $\{\mathcal{W}_x(2^m n T, 2^m), m, n \in \mathbb{Z}\}$  form the representation of  $x(t)$  with respect to the wavelet  $\psi(t)$  and the chosen grid.

Of course, we cannot assume that any set  $\psi_{mn}(t), m, n \in \mathbb{Z}$  allows reconstruction of all signals  $x(t) \in L_2(\mathbb{R})$ . For this a dual set  $\tilde{\psi}_{mn}(t), m, n \in \mathbb{Z}$  must exist, and both sets must span  $L_2(\mathbb{R})$ . The dual set need not necessarily be built from wavelets. However, we are only interested in the case where  $\tilde{\psi}_{mn}(t)$  is derived as

$$\tilde{\psi}_{mn}(t) = 2^{-\frac{m}{2}} \cdot \tilde{\psi}(2^{-m}t - nT), \quad m, n \in \mathbb{Z} \quad (8.53)$$

from a dual wavelet  $\tilde{\psi}(t)$ . If both sets  $\psi_{mn}(t)$  and  $\tilde{\psi}_{mn}(t)$  with  $m, n \in \mathbb{Z}$  span the space  $L_2(\mathbb{R})$ , any  $x(t) \in L_2(\mathbb{R})$  may be written as

$$x(t) = \sum_{m=-\infty}^{\infty} \sum_{n=-\infty}^{\infty} \langle \mathbf{x}, \psi_{mn} \rangle \tilde{\psi}_{mn}(t). \quad (8.54)$$

Alternatively, we may write  $x(t)$  as

$$x(t) = \sum_{m=-\infty}^{\infty} \sum_{n=-\infty}^{\infty} \langle \mathbf{x}, \tilde{\psi}_{mn} \rangle \psi_{mn}(t). \quad (8.55)$$

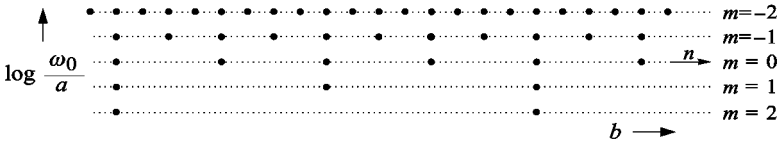


Figure 8.6. Dyadic sampling of the wavelet transform.

For a given wavelet  $\psi(t)$ , the possibility of perfect reconstruction is dependent on the sampling interval  $T$ . If  $T$  is chosen very small (oversampling), the values  $\mathcal{W}_x(2^m nT, 2^m)$ ,  $m, n \in \mathbb{Z}$  are highly redundant, and reconstruction is very easy. Then the functions  $\psi_{mn}(t)$ ,  $m, n \in \mathbb{Z}$  are linearly dependent, and an infinite number of dual sets  $\tilde{\psi}_{mn}(t)$  exists. The question of whether a dual set  $\tilde{\psi}_{mn}(t)$  exists at all can be answered by checking two frame bounds<sup>2</sup>  $A$  and  $B$ . It can be shown that the existence of a dual set and the completeness are guaranteed if the stability condition

$$A \|\mathbf{x}\|^2 \leq \sum_{m=-\infty}^{\infty} \sum_{n=-\infty}^{\infty} |\langle \mathbf{x}, \psi_{mn} \rangle|^2 \leq B \|\mathbf{x}\|^2 \tag{8.56}$$

with the frame bounds  $0 < A \leq B < \infty$  is satisfied [35]. In the case of a tight frame,  $A = B$ , perfect reconstruction with  $\tilde{\psi}_{mn}(t) = \psi_{mn}(t)$  is possible. This is also true if the samples  $\mathcal{W}_x(2^m nT, 2^m)$  contain redundancy, that is, if the functions  $\psi_{mn}(t)$ ,  $m, n \in \mathbb{Z}$  are linearly dependent. The tighter the frame bounds are, the smaller is the reconstruction error if the reconstruction is carried out according to

$$\hat{x}(t) = \frac{2}{A+B} \sum_{m=-\infty}^{\infty} \sum_{n=-\infty}^{\infty} \langle \mathbf{x}, \psi_{mn} \rangle \psi_{mn}(t). \tag{8.57}$$

If  $T$  is chosen just large enough that the samples  $\mathcal{W}_x(2^m nT, 2^m)$ ,  $m, n \in \mathbb{Z}$  contain no redundancy at all (critical sampling), the functions  $\psi_{mn}(t)$ ,  $m, n \in \mathbb{Z}$  are linearly independent. If (8.56) is also satisfied with  $0 < A \leq B < \infty$ , the functions  $\psi_{mn}(t)$ ,  $m, n \in \mathbb{Z}$  form a basis for  $L_2(\mathbb{R})$ . Then the following relation, which is known as the *biorthogonality condition*, holds:

$$\langle \psi_{mn}, \tilde{\psi}_{lk} \rangle = \delta_{ml} \delta_{nk}, \quad m, n, l, k \in \mathbb{Z}. \tag{8.58}$$

Wavelets that satisfy (8.58) are called *biorthogonal wavelets*. As a special case, we have the *orthonormal wavelets*. They are self-reciprocal and satisfy

<sup>2</sup>The problem of calculating the frame bounds will be discussed at the end of this section in detail.

the orthonormality condition

$$\langle \psi_{mn}, \psi_{lk} \rangle = \delta_{ml} \delta_{nk}, \quad m, n, l, k \in \mathbb{Z}. \tag{8.59}$$

Thus, in the orthonormal case, the functions  $\psi_{mn}(t)$ ,  $m, n \in \mathbb{Z}$  can be used for both analysis and synthesis. Orthonormal bases always have the same frame bounds (tight frame), because, in that case, (8.56) is a special form of Parseval’s relation.

### 8.4.2 Better Frequency Resolution — Decomposition of Octaves

An octave-band analysis is often insufficient. Rather, we would prefer to decompose every octave into  $M$  subbands in order to improve the frequency resolution by the factor  $M$ .

We here consider the case where the same sampling rate is used for all  $M$  subbands of an octave. This corresponds to a nesting of  $M$  dyadic wavelet analyses with the scaled wavelets

$$\psi^{(k)}(t) = 2^{\frac{k}{2M}} \psi(2^{\frac{k}{M}} t), \quad k = 0, 1, \dots, M - 1. \tag{8.60}$$

Figure 8.7 shows the sampling grid of an analysis with three voices per octave. Sampling the wavelet transform can be further generalized by choosing the sampling grid

$$a_m = a_0^m, \quad b_{mn} = a_m n T, \quad m, n \in \mathbb{Z} \tag{8.61}$$

with an arbitrary  $a_0 > 1$ . This corresponds to  $M$  nested wavelet analyses with the wavelets

$$\psi^{(k)}(t) = a_0^{\frac{k}{M}} \psi(a_0^{\frac{k}{M}} t), \quad k = 0, 1, \dots, M - 1. \tag{8.62}$$

For this general case we will list the formulae for the frame bounds  $A$  and  $B$  in (8.56) as derived by Daubechies [35]. The conditions for the validity of the formulae are:<sup>3</sup>

$$\operatorname{ess\,inf}_{|\omega| \in [1, a_0]} \sum_{m=-\infty}^{\infty} |\Psi(a_0^m \omega)|^2 > 0, \tag{8.63}$$

$$\operatorname{ess\,sup}_{|\omega| \in [1, a_0]} \sum_{m=-\infty}^{\infty} |\Psi(a_0^m \omega)|^2 < \infty, \tag{8.64}$$

and

$$\sup_{s \in \mathbb{R}} \left[ (1 + s^2)^{(1+\varepsilon)/2} \beta(s) \right] = C_\varepsilon < \infty \quad (\text{for an } \varepsilon > 0) \tag{8.65}$$

---

<sup>3</sup>By “ess inf” and “ess sup” we mean the essential infimum and supremum.

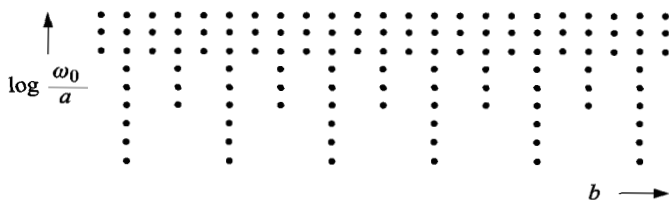


**Figure 8.7.** Sampling of the wavelet transform with three voices per octave.

with

$$\beta(s) = \sup_{|\omega| \in [1, a_0]} \sum_{m=-\infty}^{\infty} |\Psi(a_0^m \omega)| |\Psi(a_0^m \omega + s)|. \quad (8.66)$$

If (8.63) – (8.65) are satisfied for all wavelets defined in (8.62), the frame bounds  $A$  and  $B$  can be estimated on the basis of the quantities

$$c = \operatorname{ess\,inf}_{|\omega| \in [1, a_0]} \sum_{k=0}^{M-1} \sum_{m=-\infty}^{\infty} |\Psi^{(k)}(a_0^m \omega)|^2, \quad (8.67)$$

$$C = \operatorname{ess\,sup}_{|\omega| \in [1, a_0]} \sum_{k=0}^{M-1} \sum_{m=-\infty}^{\infty} |\Psi^{(k)}(a_0^m \omega)|^2, \quad (8.68)$$

$$\beta^{(k)}(s) = \sup_{|\omega| \in [1, a_0]} \sum_{m=-\infty}^{\infty} |\Psi^{(k)}(a_0^m \omega)| |\Psi^{(k)}(a_0^m \omega + s)|. \quad (8.69)$$

Provided the sampling interval  $T$  is chosen such that

$$2 \sum_{k=0}^{M-1} \sum_{\ell=1}^{\infty} \left[ \beta^{(k)} \left( \ell \frac{2\pi}{T} \right) \beta^{(k)} \left( -\ell \frac{2\pi}{T} \right) \right]^{\frac{1}{2}} < c, \quad (8.70)$$

we finally have the following estimates for  $A$  and  $B$ :

$$A \geq \frac{2\pi}{T} \left( c - 2 \sum_{k=0}^{M-1} \sum_{\ell=1}^{\infty} \left[ \beta^{(k)} \left( \ell \frac{2\pi}{T} \right) \beta^{(k)} \left( -\ell \frac{2\pi}{T} \right) \right]^{\frac{1}{2}} \right) \quad (8.71)$$

$$B \leq \frac{2\pi}{T} \left( C + 2 \sum_{k=0}^{M-1} \sum_{\ell=1}^{\infty} \left[ \beta^{(k)} \left( \ell \frac{2\pi}{T} \right) \beta^{(k)} \left( -\ell \frac{2\pi}{T} \right) \right]^{\frac{1}{2}} \right). \quad (8.72)$$

## 8.5 The Discrete Wavelet Transform (DWT)

In this section the idea of *multiresolution analysis* and the efficient realization of the discrete wavelet transform based on multirate filter banks will be addressed. This framework has mainly been developed by Meyer, Mallat and Daubechies for the orthonormal case [104, 91, 90, 34]. Since biorthogonal wavelets formally fit into the same framework [153, 36], the derivations will be given for the more general biorthogonal case.

### 8.5.1 Multiresolution Analysis

In the following we assume that the sets

$$\begin{aligned}\psi_{mn}(t) &= 2^{-\frac{m}{2}} \psi(2^{-m}t - n), \\ \tilde{\psi}_{mn}(t) &= 2^{-\frac{m}{2}} \tilde{\psi}(2^{-m}t - n),\end{aligned}\quad m, n \in \mathbb{Z} \quad (8.73)$$

are bases for  $L_2(\mathbb{R})$  satisfying the biorthogonality condition (8.58). Note that  $T = 1$  is chosen in order to simplify notation. We will mainly consider the representation (8.55) and write it as

$$x(t) = \sum_{m=-\infty}^{\infty} \sum_{n=-\infty}^{\infty} d_m(n) \psi_{mn}(t) \quad (8.74)$$

with

$$d_m(n) = \mathcal{W}_x^{\tilde{\psi}}(2^m n, 2^m) = \langle x, \tilde{\psi}_{mn} \rangle, \quad m, n \in \mathbb{Z}. \quad (8.75)$$

Since a basis consists of linearly independent functions,  $L_2(\mathbb{R})$  may be understood as the direct sum of subspaces

$$L_2(\mathbb{R}) = \dots \oplus W_{-1} \oplus W_0 \oplus W_1 \oplus \dots \quad (8.76)$$

with

$$W_m = \text{span} \{ \psi(2^{-m}t - n), n \in \mathbb{Z} \}, \quad m \in \mathbb{Z}. \quad (8.77)$$

Each subspace  $W_m$  covers a certain frequency band. For the subband signals we obtain from (8.74):

$$y_m(t) = \sum_{n=-\infty}^{\infty} d_m(n) \psi_{mn}(t), \quad y_m(t) \in W_m. \quad (8.78)$$

Every signal  $x(t) \in L_2(\mathbb{R})$  can be represented as

$$x(t) = \sum_{m=-\infty}^{\infty} y_m(t), \quad y_m(t) \in W_m. \quad (8.79)$$

Now we define the subspaces  $V_m$ ,  $m \in \mathbb{Z}$  as the direct sum of  $V_{m+1}$  and  $W_{m+1}$ :

$$V_m = V_{m+1} \oplus W_{m+1}. \quad (8.80)$$

Here we may assume that the subspaces  $V_m$  contain lowpass signals and that the bandwidth of the signals contained in  $V_m$  reduces with increasing  $m$ .

From (8.77), (8.76), and (8.80) we derive the following properties:

(i) We have a nested sequence of subspaces

$$\dots \subset V_{m+1} \subset V_m \subset V_{m-1} \subset \dots \quad (8.81)$$

(ii) Scaling of  $x(t)$  by the factor two ( $x(t) \rightarrow x(2t)$ ) makes the scaled signal  $x(2t)$  an element of the next larger subspace and vice versa:

$$x(t) \in V_m \Leftrightarrow x(2t) \in V_{m-1}. \quad (8.82)$$

(iii) If we form a sequence of functions  $x_m(t)$  by projection of  $x(t) \in L_2(\mathbb{R})$  onto the subspaces  $V_m$ , this sequence converges towards  $x(t)$ :

$$\lim_{m \rightarrow -\infty} x_m(t) = x(t), \quad x(t) \in L_2(\mathbb{R}), \quad x_m(t) \in V_m. \quad (8.83)$$

Thus, any signal may be approximated with arbitrary precision.

Because of the scaling property (8.82) we may assume that the subspaces  $V_m$  are spanned by scaled and time-shifted versions of a single function  $\phi(t)$ :

$$V_m = \text{span} \{ \phi(2^{-m}t - n), n \in \mathbb{Z} \}. \quad (8.84)$$

Thus, the subband signals  $x_m(t) \in V_m$  are expressed as

$$x_m(t) = \sum_{n=-\infty}^{\infty} c_m(n) \phi_{mn}(t) \quad (8.85)$$

with

$$\phi_{mn}(t) = 2^{-\frac{m}{2}} \phi(2^{-m}t - n). \quad (8.86)$$

The function  $\phi(t)$  is called a *scaling function*.

**Orthonormal Wavelets.** If the functions  $\psi_{mn}(t) = 2^{-\frac{m}{2}} \psi(2^{-m}t - n)$ ,  $m, n \in \mathbb{Z}$  form an orthonormal basis for  $L_2(\mathbb{R})$ , then  $L_2(\mathbb{R})$  is decomposed into an orthogonal sum of subspaces:

$$L_2(\mathbb{R}) = \dots \overset{\perp}{\oplus} W_{-1} \overset{\perp}{\oplus} W_0 \overset{\perp}{\oplus} W_1 \overset{\perp}{\oplus} \dots \quad (8.87)$$

In this case (8.80) becomes an orthogonal decomposition:

$$V_m = V_{m+1} \oplus W_{m+1}. \tag{8.88}$$

If we assume  $\|\phi\| = 1$ , then the functions

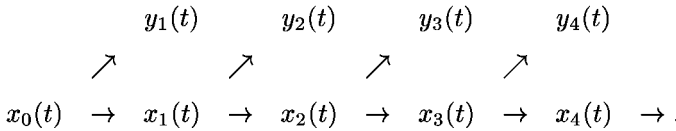
$$\phi_{mn}(t) = 2^{-\frac{m}{2}} \phi(2^{-m}t - n), \quad m, n \in \mathbb{Z}, \tag{8.89}$$

form orthonormal bases for the spaces  $V_m$ ,  $m \in \mathbb{Z}$ .

**Signal Decomposition.** From (8.80) we derive

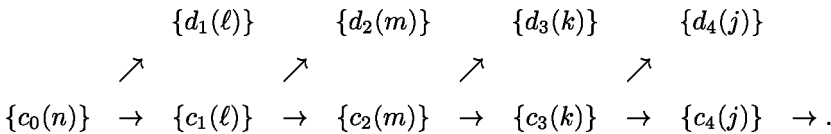
$$x_m(t) = x_{m+1}(t) + y_{m+1}(t). \tag{8.90}$$

If we assume that one of the signals  $x_m(t)$ , for example  $x_0(t)$ , is known, this signal can be successively decomposed according to (8.90):



The signals  $y_1(t), y_2(t), \dots$  contain the high-frequency components of  $x_0(t), x_1(t)$ , etc., so that the decomposition is a successive lowpass filtering accompanied by separating bandpass signals. Since the successive lowpass filtering results in an increasing loss of detail information, and since these details are contained in  $y_1(t), y_2(t), \dots$  we also speak of a multiresolution analysis (MRA).

Assuming a known sequence  $\{c_0(n)\}$ , the sequences  $\{c_m(n)\}$  and  $\{d_m(n)\}$  for  $m > 0$  may also be derived directly according to the scheme



In the next section we will discuss this very efficient method in greater detail.

**Example: Haar Wavelets.** The *Haar function* is the simplest example of an orthonormal wavelet:

$$\psi(t) = \begin{cases} 1 & \text{for } 0 \leq t < 0.5 \\ -1 & \text{for } 0.5 \leq t < 1 \\ 0 & \text{otherwise.} \end{cases}$$

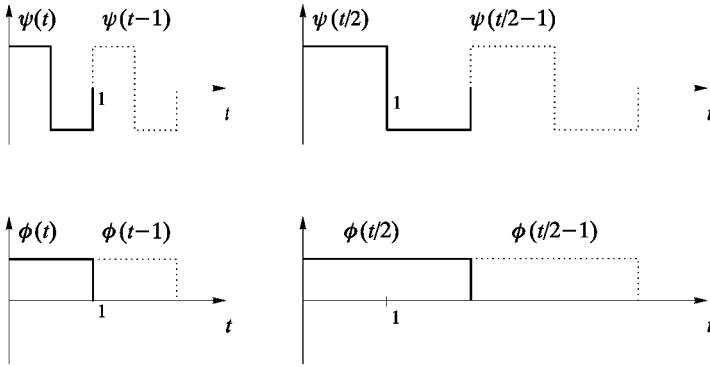


**Figure 8.8.** Haar wavelet and scaling function.

The corresponding scaling function is

$$\phi(t) = \begin{cases} 1, & \text{for } 0 \leq t < 1 \\ 0, & \text{otherwise.} \end{cases}$$

The functions  $\psi(t - n)$ ,  $n \in \mathbb{Z}$  span the subspace  $W_0$ , and the functions  $\psi(\frac{1}{2}t - n)$ ,  $n \in \mathbb{Z}$  span  $W_1$ . Furthermore, the functions  $\phi(t - n)$ ,  $n \in \mathbb{Z}$  span  $V_0$  and the functions  $\phi(\frac{1}{2}t - n)$ ,  $n \in \mathbb{Z}$  span  $V_1$ . The orthogonality among the basis functions  $\psi(2^{-m}t - n)$ ,  $m, n \in \mathbb{Z}$  and the orthogonality of the functions  $\psi(2^{-m}t - n)$ ,  $m, n \in \mathbb{Z}$  and  $\phi(2^{-j}t - n)$ ,  $j \geq m$  is obvious, see Figure 8.8.

**Example: Shannon Wavelets.** The *Shannon wavelets* are impulse responses of ideal bandpass filters:

$$\psi(t) = \frac{\sin \frac{\pi}{2}t}{\frac{\pi}{2}t} \cos \frac{3\pi}{2}t. \tag{8.91}$$

In the frequency domain this is

$$\Psi(\omega) = \begin{cases} 1 & \text{for } \pi \leq |\omega| \leq 2\pi, \\ 0 & \text{otherwise.} \end{cases} \tag{8.92}$$

The scaling function that belongs to the Shannon wavelet is the impulse response of the ideal lowpass:

$$\phi(t) = \frac{\sin \pi t}{\pi t} \tag{8.93}$$

$$\updownarrow \tag{8.94}$$

$$\Phi(\omega) = \begin{cases} 1 & \text{for } 0 \leq |\omega| \leq \pi, \\ 0 & \text{otherwise.} \end{cases} \tag{8.95}$$

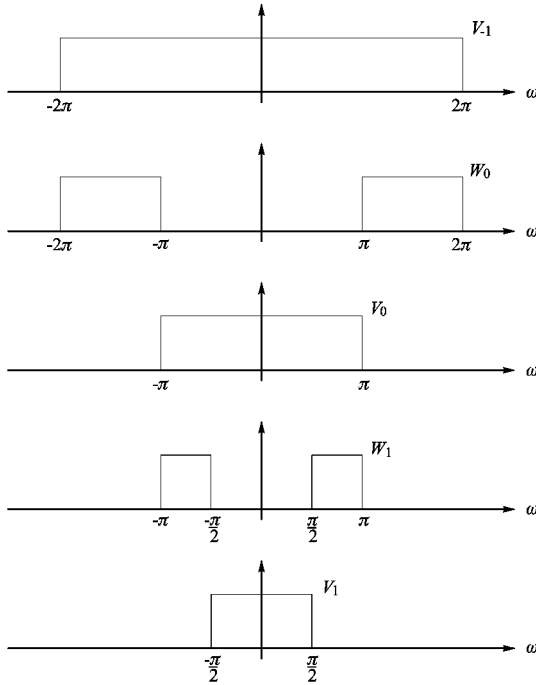


**Figure 8.9.** Subspaces of Shannon wavelets.

The coefficients  $c_m(n)$ ,  $m, n \in \mathbb{Z}$  in (8.85) can be understood as the sample values of the ideally lowpass-filtered signal. Figure 8.9 illustrates the decomposition of the signal space.

The Shannon wavelets form an orthonormal basis for  $L_2(\mathbb{R})$ . The orthogonality between different scales is easily seen, because the spectra do not overlap. For the inner product of translated versions of  $\phi(t)$  at the same scale, we get

$$\begin{aligned}
 \int_{-\infty}^{\infty} \phi(t - m)\phi^*(t - n) &= \frac{1}{2\pi} \int_{-\pi}^{\pi} \Phi(\omega)\Phi^*(\omega)e^{-j(m - n)\omega} d\omega \\
 &= \frac{1}{2\pi} \int_{-\pi}^{\pi} e^{-j(m - n)\omega} d\omega \qquad (8.96) \\
 &= \delta_{mn}
 \end{aligned}$$

by using Parseval’s relation. The orthogonality of translated wavelets at the same scale is shown using a similar derivation.

A drawback of the Shannon wavelets is their infinite support and the

poor time resolution due to the slow decay. On the other hand, the frequency resolution is perfect. For the Haar wavelets, we observed the opposite behavior. They had perfect time, but unsatisfactory frequency resolution.

### 8.5.2 Wavelet Analysis by Multirate Filtering

Because of  $V_0 = V_1 \oplus W_1$  the functions  $\phi_{0n}(t) = \phi(t - n) \in V_0$ ,  $n \in \mathbb{Z}$  can be written as linear combinations of the basis functions for the spaces  $V_1$  and  $W_1$ . With the coefficients  $h_0(2\ell - n)$  and  $h_1(2\ell - n)$ ,  $\ell, n \in \mathbb{Z}$  the approach is

$$\phi_{0n}(t) = \sum_{\ell} h_0(2\ell - n) \phi_{1\ell}(t) + h_1(2\ell - n) \psi_{1\ell}(t). \quad (8.97)$$

Equation (8.97) is known as the *decomposition relation*, for which the following notation is used as well:

$$\sqrt{2} \phi(2t - n) = \sum_{\ell} h_0(2\ell - n) \phi(t - \ell) + h_1(2\ell - n) \psi(t - \ell). \quad (8.98)$$

We now consider a known sequence  $\{c_0(n)\}$ , and we substitute (8.97) into (8.85) for  $m = 0$ . We get

$$\begin{aligned} x_0(t) &= \sum_n c_0(n) \phi_{0n}(t) \\ &= \sum_n c_0(n) \sum_{\ell} h_0(2\ell - n) \phi_{1\ell}(t) + h_1(2\ell - n) \psi_{1\ell}(t) \\ &= \sum_{\ell} \underbrace{\sum_n c_0(n) h_0(2\ell - n)}_{c_1(\ell)} \phi_{1\ell}(t) + \sum_{\ell} \underbrace{\sum_n c_0(n) h_1(2\ell - n)}_{d_1(\ell)} \psi_{1\ell}(t) \\ &= x_1(t) + y_1(t), \end{aligned} \quad (8.99)$$

where  $x_0 \in V_0$ ,  $x_1 \in V_1$ , and  $y_1 \in W_1$ . This method allows us to compute  $\{c_{m+1}(\ell)\}$  and  $\{d_{m+1}(\ell)\}$  from  $\{c_m(n), m, n \in \mathbb{Z}\}$ :

$$\left. \begin{aligned} c_{m+1}(\ell) &= \sum_n c_m(n) h_0(2\ell - n) \\ d_{m+1}(\ell) &= \sum_n c_m(n) h_1(2\ell - n) \end{aligned} \right\}, \quad i, \ell \in \mathbb{Z}. \quad (8.100)$$

We see that the sequences  $\{c_{m+1}(\ell)\}$  and  $\{d_{m+1}(\ell)\}$  occur with half the sampling rate of  $\{c_m(n)\}$ . Altogether, the decomposition (8.100) is equivalent to a two-channel filter bank analysis with the analysis filters  $h_0(n)$  and  $h_1(n)$ .

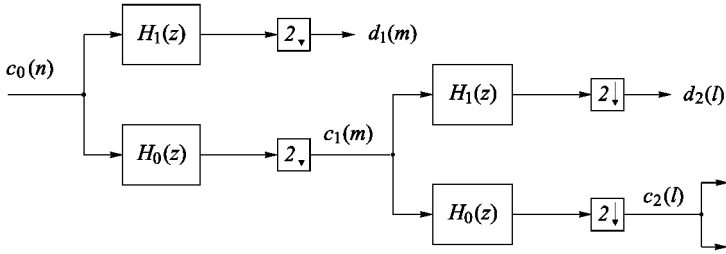


**Figure 8.10.** Analysis filter bank for computing the DWT.

If we assume that  $x_0(t)$  is a sufficiently good approximation of  $x(t)$ , and if we know the coefficients  $c_0(n)$ , we are able to compute the coefficients  $c_{m+1}(n)$ ,  $d_{m+1}(n)$ ,  $m > 0$ , and thus the values of the wavelet transform using the discrete-time filter bank depicted in Figure 8.10. This is the most efficient way of computing the DWT of a signal.

### 8.5.3 Wavelet Synthesis by Multirate Filtering

Let us consider two sequences  $g_0(n)$  and  $g_1(n)$ , which allow us to express the functions  $\phi_{10}(t) = 2^{-1/2}\phi(t/2) \in V_1$  and  $\psi_{10}(t) = 2^{-1/2}\psi(t/2) \in W_1$  as linear combinations of  $\phi_{0n}(t) = \phi(t - n) \in V_0$ ,  $n \in \mathbb{Z}$  in the form

$$\begin{aligned} \phi_{10}(t) &= \sum_n g_0(n) \phi_{0n}(t), \\ \psi_{10}(t) &= \sum_n g_1(n) \phi_{0n}(t), \end{aligned} \tag{8.101}$$

or equivalently as

$$\begin{aligned} \phi(t) &= \sum_n g_0(n) \sqrt{2} \phi(2t - n), \\ \psi(t) &= \sum_n g_1(n) \sqrt{2} \phi(2t - n). \end{aligned} \tag{8.102}$$

Equations (8.101) and (8.102), respectively, are referred to as the *two-scale relation*. For time-shifted functions the two-scale relation is

$$\begin{aligned} \phi_{1\ell}(t) &= \sum_n g_0(n - 2\ell) \phi_{0n}(t), \\ \psi_{1\ell}(t) &= \sum_n g_1(n - 2\ell) \phi_{0n}(t). \end{aligned} \tag{8.103}$$

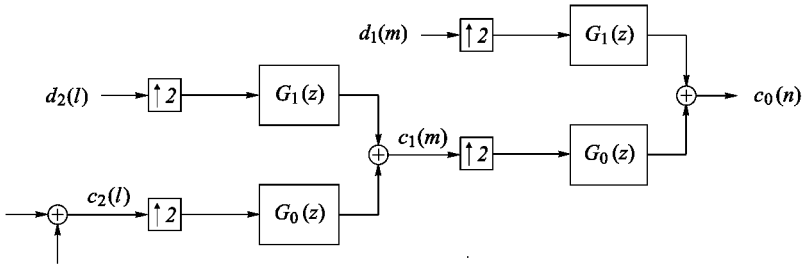


Figure 8.11. Synthesis filter bank.

From (8.103), (8.78), (8.85) and (8.90) we derive

$$\begin{aligned}
 x_0(t) &= x_1(t) + y_1(t) \\
 &= \sum_{\ell} c_1(\ell) \phi_{1\ell}(t) + \sum_{\ell} d_1(\ell) \psi_{1\ell}(t) \\
 &= \sum_{\ell} c_1(\ell) \sum_n g_0(n - 2\ell) \phi_{0n}(t) + \sum_{\ell} d_1(\ell) \sum_n g_1(n - 2\ell) \phi_{0n}(t) \\
 &= \sum_n \left( \sum_{\ell} c_1(\ell) g_0(n - 2\ell) + d_1(\ell) g_1(n - 2\ell) \right) \phi_{0n}(t) \\
 &= \sum_n c_0(n) \phi_{0n}(t).
 \end{aligned}
 \tag{8.104}$$

The generalization of (8.104) yields

$$c_m(n) = \sum_{\ell} c_{m+1}(\ell) g_0(n - 2\ell) + d_{m+1}(\ell) g_1(n - 2\ell).
 \tag{8.105}$$

The sequences  $g_0(n)$  and  $g_1(n)$  may be understood as the impulse responses of discrete-time filters, and (8.105) describes a discrete-time two-channel synthesis filter bank. The filter bank is shown in Figure 8.11.

### 8.5.4 The Relationship between Filters and Wavelets

Let us consider the decomposition relation (8.97), that is

$$\phi_{0n}(t) = \sum_{\ell} h_0(2\ell - n) \phi_{1\ell}(t) + h_1(2\ell - n) \psi_{1\ell}(t).
 \tag{8.106}$$

Taking the inner product of (8.106) with  $\tilde{\phi}_{1\ell}(t)$  and  $\tilde{\psi}_{1\ell}(t)$  yields

$$\begin{aligned}\langle \phi_{0n}, \tilde{\phi}_{1\ell} \rangle &= \sum_m h_0(2m-n) \langle \phi_{1m}, \tilde{\phi}_{1\ell} \rangle + h_1(2m-n) \langle \psi_{1m}, \tilde{\phi}_{1\ell} \rangle, \\ \langle \phi_{0n}, \tilde{\psi}_{1\ell} \rangle &= \sum_m h_0(2m-n) \langle \phi_{1m}, \tilde{\psi}_{1\ell} \rangle + h_1(2m-n) \langle \psi_{1m}, \tilde{\psi}_{1\ell} \rangle.\end{aligned}\tag{8.107}$$

Observing that

$$\begin{aligned}\langle \phi_{1m}, \tilde{\phi}_{1\ell} \rangle &= \delta_{\ell m}, \\ \langle \psi_{1m}, \tilde{\psi}_{1\ell} \rangle &= \delta_{\ell m}, \\ \langle \phi_{1m}, \tilde{\psi}_{1\ell} \rangle &= 0, \\ \langle \psi_{1m}, \tilde{\phi}_{1\ell} \rangle &= 0,\end{aligned}\tag{8.108}$$

we obtain

$$\begin{aligned}h_0(2\ell-n) &= \langle \phi_{0n}, \tilde{\phi}_{1\ell} \rangle, \\ h_1(2\ell-n) &= \langle \phi_{0n}, \tilde{\psi}_{1\ell} \rangle.\end{aligned}\tag{8.109}$$

Similarly, the two-scale relation (8.101) yields

$$\begin{aligned}g_0(n) &= \langle \phi_{10}, \tilde{\phi}_{0n} \rangle, \\ g_1(n) &= \langle \psi_{10}, \tilde{\phi}_{0n} \rangle.\end{aligned}\tag{8.110}$$

Substituting (8.101) into (8.108) yields

$$\begin{aligned}\delta_{\ell 0} &= \sum_n g_0(n) \langle \phi_{0n}, \tilde{\phi}_{1\ell} \rangle, \\ \delta_{\ell 0} &= \sum_n g_1(n) \langle \phi_{0n}, \tilde{\psi}_{1\ell} \rangle, \\ 0 &= \sum_n g_0(n) \langle \phi_{0n}, \tilde{\psi}_{1\ell} \rangle, \\ 0 &= \sum_n g_1(n) \langle \phi_{0n}, \tilde{\phi}_{1\ell} \rangle,\end{aligned}\tag{8.111}$$

and by comparing (8.111) with (8.109) we obtain

$$\begin{aligned}\delta_{\ell 0} &= \sum_n g_0(n) h_0(2\ell-n), \\ \delta_{\ell 0} &= \sum_n g_1(n) h_1(2\ell-n), \\ 0 &= \sum_n g_0(n) h_1(2\ell-n), \\ 0 &= \sum_n g_1(n) h_0(2\ell-n).\end{aligned}\tag{8.112}$$

The conditions (8.112) are nothing but the PR conditions for critically subsampled two-channel filter banks, formulated in the time domain, cf. Section 6.2. By  $z$ -transform of (8.112) we obtain

$$\begin{aligned} 2 &= G_0(z) H_0(z) + G_0(-z) H_0(-z), \\ 2 &= G_1(z) H_1(z) + G_1(-z) H_1(-z), \\ 0 &= G_0(z) H_1(z) + G_0(-z) H_1(-z), \\ 0 &= G_1(z) H_0(z) + G_1(-z) H_0(-z). \end{aligned} \tag{8.113}$$

**Orthonormal Wavelets.** If the sets  $\phi_{mn}(t)$  and  $\psi_{mn}(t)$ ,  $m, n \in \mathbb{Z}$  according to (8.51) and (8.89) are orthonormal bases for  $V_m$  and  $W_m$ ,  $m \in \mathbb{Z}$ , (8.109) becomes

$$\begin{aligned} h_0(2\ell - n) &= \langle \phi_{0n}, \phi_{1\ell} \rangle, \\ h_1(2\ell - n) &= \langle \phi_{0n}, \psi_{1\ell} \rangle. \end{aligned} \tag{8.114}$$

Substituting the two-scale relation (8.103) into (8.114) yields

$$\begin{aligned} h_0(2\ell - n) &= \sum_k g_0^*(k - 2\ell) \langle \phi_{0n}, \phi_{0k} \rangle, \\ h_1(2\ell - n) &= \sum_k g_1^*(k - 2\ell) \langle \phi_{0n}, \phi_{0k} \rangle. \end{aligned} \tag{8.115}$$

Observing  $\langle \phi_{0n}, \phi_{0k} \rangle = \delta_{nk}$ , we derive

$$\begin{aligned} h_0(n) &= g_0^*(-n) \iff H_0(z) = \tilde{G}_0(z), \\ h_1(n) &= g_1^*(-n) \iff H_1(z) = \tilde{G}_1(z). \end{aligned} \tag{8.116}$$

Thus equations (8.112) and (8.113) become

$$\begin{aligned} \delta_{\ell 0} &= \sum_n g_0(n) g_0^*(n - 2\ell), \\ \delta_{\ell 0} &= \sum_n g_1(n) g_1^*(n - 2\ell), \\ 0 &= \sum_n g_0(n) g_1^*(n - 2\ell), \\ 0 &= \sum_n g_1(n) g_0^*(n - 2\ell) \end{aligned} \tag{8.117}$$

and

$$\begin{aligned} 2 &= G_0(z) \tilde{G}_0(z) + G_0(-z) \tilde{G}_0(-z), \\ 2 &= G_1(z) \tilde{G}_1(z) + G_1(-z) \tilde{G}_1(-z), \\ 0 &= G_0(z) \tilde{G}_1(z) + G_0(-z) \tilde{G}_1(-z), \\ 0 &= G_1(z) \tilde{G}_0(z) + G_1(-z) \tilde{G}_0(-z). \end{aligned} \tag{8.118}$$

These are nothing but the requirements for paraunitary two-channel filter banks, as derived in Chapter 6.

## 8.6 Wavelets from Filter Banks

### 8.6.1 General Procedure

In the previous sections we assumed that the wavelets and scaling functions are given. Due to the properties of the wavelet transform we were able to show the existence of sequences  $h_0(n)$ ,  $h_1(n)$ ,  $g_0(n)$ , and  $g_1(n)$ , which allow us to realize the transform via a multirate filter bank. When constructing wavelets and scaling functions one often adopts the reverse strategy. One chooses the coefficients of a PR two-channel filter bank in such a way that the wavelets and scaling functions associated with these filters have the desired properties.

**Scaling Function.** The starting point for constructing scaling functions is the first part of the two-scale relation (8.102):

$$\phi(t) = \sum_n g_0(n) \sqrt{2} \phi(2t - n). \quad (8.119)$$

In the following the Fourier transform of equation (8.119) is required, which, using

$$\phi(2t - n) \longleftrightarrow \frac{1}{2} \Phi\left(\frac{\omega}{2}\right) e^{-\frac{j\omega n}{2}}, \quad (8.120)$$

is

$$\Phi(\omega) = \Phi\left(\frac{\omega}{2}\right) \frac{1}{\sqrt{2}} \sum_n g_0(n) e^{-\frac{j\omega n}{2}}. \quad (8.121)$$

With

$$G_0(e^{j\frac{\omega}{2}}) = \sum_n g_0(n) e^{-\frac{j\omega n}{2}} \quad (8.122)$$

equation (8.121) is

$$\Phi(\omega) = \frac{1}{\sqrt{2}} G_0(e^{j\frac{\omega}{2}}) \Phi\left(\frac{\omega}{2}\right). \quad (8.123)$$

Since the scaling function  $\phi(t)$  is supposed to be a lowpass impulse response, we may introduce the normalization

$$\Phi(0) = \int_{-\infty}^{\infty} \phi(t) dt = 1. \quad (8.124)$$

If we now apply (8.119) and (8.123)  $K$  times, we obtain

$$\Phi(\omega) = \left( \prod_{k=1}^K \frac{1}{\sqrt{2}} G_0(e^{j\omega/2^k}) \right) \Phi\left(\frac{\omega}{2^K}\right). \quad (8.125)$$

Now we let  $K \rightarrow \infty$ . If the product in (8.125) converges for  $K \rightarrow \infty$  to a continuous function, it converges to

$$\Phi(\omega) = \prod_{k=1}^{\infty} \frac{1}{\sqrt{2}} G_0(e^{j\omega/2^k}), \quad (8.126)$$

because we have specified  $\Phi(0) = 1$ . Thus (8.119) allows us to determine the scaling function recursively. When starting with

$$x_0(t) = \begin{cases} 1 & \text{for } 0 \leq t < 1, \\ 0 & \text{otherwise,} \end{cases} \quad (8.127)$$

we obtain the piecewise constant functions  $x_i(t)$  by means of the recursion

$$x_{i+1}(t) = \sqrt{2} \sum_n g_0(n) x_i(2t - n), \quad (8.128)$$

which approaches the scaling function for  $i \rightarrow \infty$ .

Figure 8.12 illustrates the recursive calculation of the scaling function  $\phi(t)$ . However, the convergence of the product does not guarantee that the obtained scaling function is smooth. Figures 8.13 and 8.14 show examples leading to smooth and fractal scaling functions, respectively.

**Wavelet.** If the scaling function  $\phi(t)$  is known,  $\psi(t)$  can be calculated by using the second part of the two-scale relation (8.102):

$$\psi(t) = \sum_n g_1(n) \sqrt{2} \phi(2t - n). \quad (8.129)$$

It is obvious that a smooth  $\phi(t)$  results in a smooth  $\psi(t)$ , regardless of the coefficients  $g_1(n)$ , so that all concerns regarding smoothness are related to the lowpass  $g_0(n)$ .

**Summary of Construction Formulae.** According to (8.126), the synthesis scaling function is related to the synthesis lowpass as

$$\Phi(\omega) = \prod_{k=1}^{\infty} \frac{1}{\sqrt{2}} G_0(e^{j\omega/2^k}). \quad (8.130)$$

For the synthesis wavelet we get from (8.129) and (8.130)

$$\Psi(\omega) = \frac{1}{\sqrt{2}} G_1(e^{j\omega/2}) \prod_{k=2}^{\infty} \frac{1}{\sqrt{2}} G_0(e^{j\omega/2^k}). \quad (8.131)$$

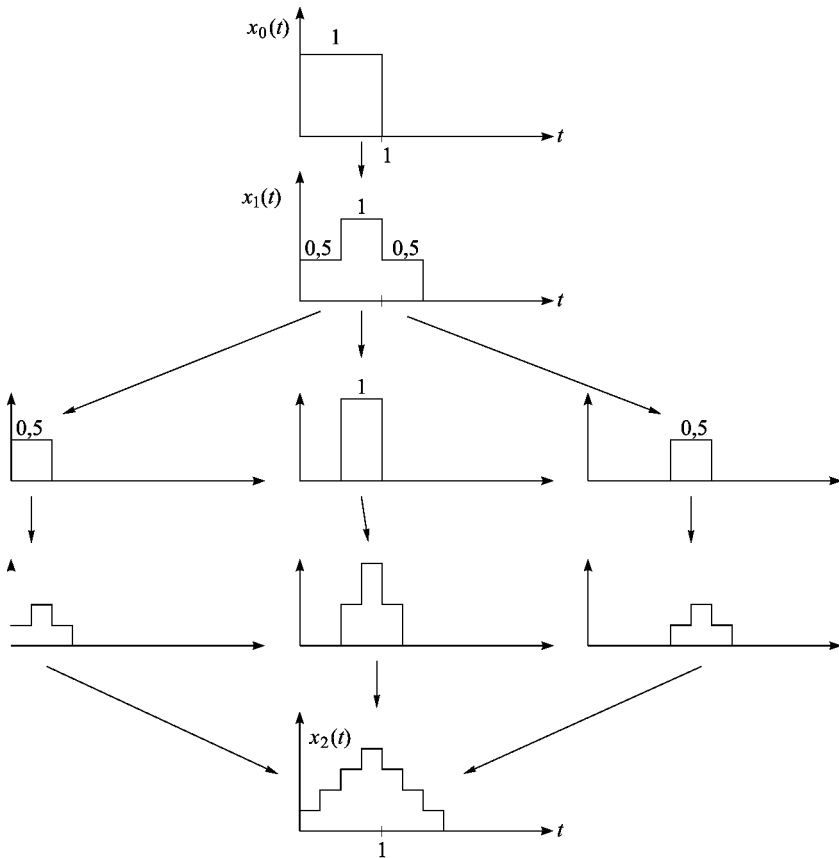


**Figure 8.12.** Recursive calculation of the scaling function  $\phi(t)$ ; the first two steps of the recursion are shown (coefficients:  $\{g_0(n)\} = \frac{\sqrt{2}}{2} \{\frac{1}{2}, 1, \frac{1}{2}\}$ ).

The analysis scaling function  $\tilde{\phi}(t)$  and the wavelet  $\tilde{\psi}(t)$  are related to the time-reversed and complex conjugated analysis filters  $h_0^*(-n)$  and  $h_1^*(-n)$  in the same way as  $\phi(t)$  and  $\psi(t)$  are related to  $g_0(n)$  and  $g_1(n)$ . Thus, they may be given in the frequency domain as

$$\tilde{\Phi}(\omega) = \prod_{k=1}^{\infty} \frac{1}{\sqrt{2}} H_0(e^{-j\omega/2^k}) \tag{8.132}$$

and

$$\tilde{\Psi}(\omega) = \frac{1}{\sqrt{2}} H_1(e^{-j\omega/2}) \prod_{k=2}^{\infty} \frac{1}{\sqrt{2}} H_0(e^{-j\omega/2^k}). \tag{8.133}$$

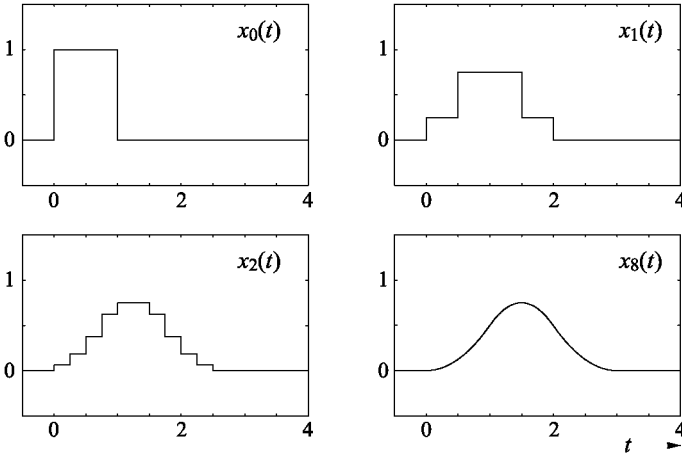


**Figure 8.13.** Recursive calculation of the scaling function  $\phi(t)$  (coefficients  $\{g_0(n)\} = \frac{\sqrt{2}}{8}\{1\ 3\ 3\ 1\}$ ).

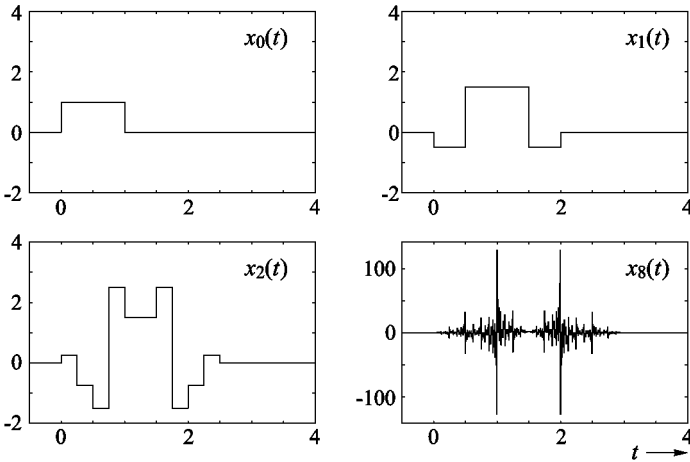


**Figure 8.14.** Recursive calculation of the scaling function  $\phi(t)$  (coefficients  $\{g_0(n)\} = \frac{\sqrt{2}}{4}\{-1\ 3\ 3\ -1\}$ ).

**Non-Linear Phase Property of Orthonormal Wavelets.** In Chapter 6 we have shown that paraunitary two-channel filter banks have non-linear phase filters in general. This property is transferred directly to the scaling functions and wavelets constructed with these filters. Thus, orthonormal wavelets have non-linear phase in general. Exceptions are the Haar and Shannon wavelets.

### 8.6.2 Requirements to be Met by the Coefficients

We have already shown that to construct biorthogonal and orthonormal scaling functions and wavelets the coefficients of PR two-channel filter banks are required. But, in order to satisfy (8.124), the coefficients must be scaled appropriately. The correct scaling for the lowpass can be found by integrating (8.119):

$$\int_{-\infty}^{\infty} \phi(t) dt = \frac{1}{\sqrt{2}} \sum_n g_0(n) \int_{-\infty}^{\infty} \phi(2t - n) d(2t). \quad (8.134)$$

This yields

$$\sum_n g_0(n) = \sqrt{2}. \quad (8.135)$$

By integrating equation (8.129) we obtain

$$\int_{-\infty}^{\infty} \psi(t) dt = \frac{1}{\sqrt{2}} \sum_n g_1(n) \int_{-\infty}^{\infty} \phi(2t - n) d(2t), \quad (8.136)$$

and with (8.124) and  $\int \psi(t) dt = 0$  we conclude

$$\sum_n g_1(n) = 0. \quad (8.137)$$

This means that the highpass filters in the two-channel filter bank must have zero mean in order to allow the construction of wavelets.

### 8.6.3 Partition of Unity

In order to enforce a lowpass characteristic of  $G_0(z)$ , it is useful to require

$$G_0(-1) = 0 \iff \sum_n (-1)^n g_0(n) = 0. \quad (8.138)$$

As will be shown in the following, (8.135), (8.135), and (8.138) result in

$$\Phi(2\pi k) = \begin{cases} 1 & k = 0 \\ 0 & k \neq 0. \end{cases} \quad (8.139)$$

In the time domain, this property of the scaling function, which is known as the partition of unity, is written

$$\sum_{n=-\infty}^{\infty} \phi(t - n) = 1. \quad (8.140)$$

*Proof of (8.139).* We consider (8.123) for  $\omega = 2\pi k$ , observing (8.135) and (8.138):

$$\begin{aligned}\Phi(2\pi k) &= \frac{1}{\sqrt{2}}G_0(e^{j\pi k})\Phi(\pi k) \\ &= \frac{1}{\sqrt{2}}G_0((-1)^k)\Phi(\pi k) \\ &= \begin{cases} \Phi(\pi k) & k \text{ even,} \\ 0 & k \text{ odd.} \end{cases}\end{aligned}\tag{8.141}$$

For  $k = 0, 1, 2, 3, 4, \dots$  we obtain

$$\begin{aligned}k = 0: \quad \Phi(0) &= \Phi(0) &= 1, \\ k = 1: \quad \Phi(2\pi) &= 0 \cdot \Phi(\pi) &= 0, \\ k = 2: \quad \Phi(4\pi) &= 1 \cdot \Phi(2\pi) &= 0, \\ k = 3: \quad \Phi(6\pi) &= 0 \cdot \Phi(3\pi) &= 0, \\ k = 4: \quad \Phi(8\pi) &= 1 \cdot \Phi(4\pi) &= 0, \\ &\vdots &\vdots\end{aligned}\tag{8.142}$$

We may proceed in a similar way for the negative indices, and it turns out that (8.139) holds.  $\square$

### 8.6.4 The Norm of Constructed Scaling Functions and Wavelets

When the coefficients  $g_0(n)$  belong to a paraunitary filter bank, (8.124) directly leads to

$$\|\phi\| = 1.\tag{8.143}$$

We realize this by forming the inner product of (8.140) with  $\phi_{00}(t)$  and by making use of orthogonality:

$$\underbrace{\langle \phi_{00}, \sum_{n=-\infty}^{\infty} \phi_{0n} \rangle}_{\langle \phi_{00}, \phi_{00} \rangle} = \underbrace{\langle \phi_{00}, \mathbf{1} \rangle}_{\Phi(0)=1}.\tag{8.144}$$

Forming the inner product  $\langle \psi_{00}, \psi_{00} \rangle$  by using (8.101) yields

$$\begin{aligned}\langle \psi_{00}, \psi_{00} \rangle &= \langle \sum_k g_1(k) \phi_{1k}, \sum_n g_1(n) \phi_{1n} \rangle \\ &= \sum_k \sum_n g_1(k) g_1^*(n) \underbrace{\langle \phi_{1k}, \phi_{1n} \rangle}_{\delta_{nk}} = \|\mathbf{g}_1\|^2 = 1,\end{aligned}\tag{8.145}$$

which shows that

$$\|\psi\| = 1 \quad (8.146)$$

for the norm of the wavelet  $\psi(t)$ . Assuming  $\Phi(0) = \alpha$  leads to  $\|\phi\| = \|\psi\| = \alpha$ .

In the biorthogonal case the relationship between the norm of the coefficients and the norm of the scaling function is much more complicated.

### 8.6.5 Moments

Multiresolution signal decompositions are often carried out in order to compress signals, so that the compaction properties of such decompositions are of crucial importance. Most signals to be compressed are of a lowpass nature and can be well approximated locally by low-order polynomials. Therefore, it is useful to seek wavelets with good approximation properties for low-order polynomials. As we shall see, the approximation properties of a multiresolution decomposition are intimately related to the number of vanishing wavelet moments.

The  $k$ th moment of a wavelet  $\psi(t)$  is given by

$$m_k = \int_{-\infty}^{\infty} t^k \psi(t) dt. \quad (8.147)$$

Using the property (2.40) of the Fourier transform, the moments can also be expressed as

$$m_k = (-j)^{-k} \left. \frac{d^k \Psi(\omega)}{d\omega^k} \right|_{\omega=0} \quad (8.148)$$

Thus, if  $\Psi(\omega)$  has  $N_\psi$  zeros at  $\omega = 0$ , the wavelet has  $N_\psi$  vanishing moments, that is

$$\int_{-\infty}^{\infty} t^k \psi(t) dt = 0 \quad \text{for } k = 0, 1, \dots, N_\psi - 1. \quad (8.149)$$

Clearly, the inner product of an analysis wavelet  $\tilde{\psi}(t)$  having  $N_{\tilde{\psi}}$  vanishing moments with a signal

$$x(t) = \sum_{k=0}^{N_{\tilde{\psi}}-1} a_k t^k$$

is zero, and, consequently, all wavelet coefficients are zero. Thus, polynomial signals of order  $N_{\tilde{\psi}} - 1$  are solely represented by the lowpass component, that is, by the coefficients of the scaling function.

The number of vanishing moments is easily controlled when constructing wavelets from filter banks. In order to see this, let us recall equation (8.133):

$$\tilde{\Psi}(\omega) = \frac{1}{\sqrt{2}} H_1(e^{-j\omega/2}) \prod_{k=2}^{\infty} \frac{1}{\sqrt{2}} H_0(e^{-j\omega/2^k}). \quad (8.150)$$

$N_{\tilde{\psi}}$  is given by the number of zeros of  $H_1(e^{j\omega})$  at  $\omega = 0$ , or, equivalently, by the number of zeros of  $H_1(z)$  at  $z = 1$ . Note that according to (6.22),  $H_1(z)$  is a modulated version of the synthesis lowpass  $G_0(z)$ , so that we may alternatively say that  $N_{\tilde{\psi}}$  is given by the number of zeros of  $G_0(z)$  at  $z = -1$ . Similarly, the number of vanishing moments of the synthesis wavelet is equal to the number of zeros of the analysis lowpass at  $z = -1$ .

The discrete-time filters also have vanishing moments and corresponding approximation properties for discrete-time polynomial signals. For the  $k$ th derivative of

$$H_1(e^{j\omega}) = \sum_n h_1(n) e^{-j\omega n} \quad (8.151)$$

we get

$$\frac{d^k H_1(e^{j\omega})}{d\omega^k} = \sum_n (-jn)^k h_1(n) e^{-j\omega n}. \quad (8.152)$$

From this expression we see that if  $H_1(z)$  has  $N_{\tilde{\psi}}$  zeros at  $z = 1$ , then  $h_1(n)$  has  $N_{\tilde{\psi}}$  vanishing moments in the discrete-time sense:

$$\sum_n n^k h_1(n) = 0 \quad \text{for } k = 0, 1, \dots, N_{\tilde{\psi}} - 1. \quad (8.153)$$

This means that sampled polynomial signals of order  $N_{\tilde{\psi}} - 1$  are solely represented by the lowpass component.

## 8.6.6 Regularity

In Figures 8.13 and 8.14 we saw that different filters may have completely different convergence properties. Typically, one prefers smooth functions  $\phi(t)$ , which should possibly have several continuous derivatives. Daubechies derived a test that can check the regularity and thus the convergence of the product in (8.125) [34]. Assuming that  $G_0(z)$  has  $N$  zeros at  $z = -1$ ,  $G_0(z)$  can be written as

$$G_0(z) = \sqrt{2} \left( \frac{1+z^{-1}}{2} \right)^N S(z). \quad (8.154)$$

Note that  $N \geq 1$  because of (8.137). Further note that  $S(1) = 1$  because of (8.135). Pointwise convergence of the functions  $x_i(t)$  defined in (8.128)

towards a continuous function  $x_\infty(t) = \phi(t)$  is guaranteed if

$$\sup_{0 \leq \omega \leq 2\pi} |S(e^{j\omega})| < 2^{N-1}. \tag{8.155}$$

Clearly, if  $G_0(z)$  has no zero at  $z = -1$ , then (8.155) cannot be satisfied because  $S(1) = 1$ .

If  $N$  is larger than the minimum number that is required to satisfy (8.155), then the function  $\phi(t)$  will also have continuous derivatives. Precisely,  $\phi(t)$  is  $m$ -times continuously differentiable if

$$\sup_{0 \leq \omega \leq 2\pi} |S(e^{j\omega})| < 2^{N-m-1}. \tag{8.156}$$

Regularity is only associated with the lowpass filters  $g_0(n)$  and  $h_0(n)$ , respectively. Given a continuous function  $\phi(t)$ , the function  $\psi(t)$  according to (8.129) will be continuous for any sequence  $g_1(n)$ .

**Hölder Regularity.** Rioul introduced the concept of Hölder regularity, which can be expressed as follows: if a scaling function is  $m$ -times continuously differentiable and its  $m$ th derivative  $\psi^{(m)}(t)$  is Hölder continuous of order  $\alpha$ , then its regularity is  $r = m + \alpha$  [125]. The Hölder exponent  $\alpha$  is the maximum  $\alpha$  for which

$$|\psi^{(m)}(t) - \psi^{(m)}(t + \tau)| \leq C |\tau|^\alpha \quad \forall t, \tau \tag{8.157}$$

### 8.6.7 Wavelets with Finite Support

If  $g_0(n)$  and  $g_1(n)$  are FIR filters, then the resulting scaling functions and wavelets have finite support [34]. The proof is straightforward. One merely has to consider the iteration (8.128) with the  $L$  coefficients  $g_0(0), \dots, g_0(L-1)$  while assuming that  $x_i(t)$  is restricted to the interval  $[0, L-1]$ :

$$x_{i+1}(t) = \sqrt{2} \sum_{n=0}^{L-1} g_0(n) x_i(2t - n). \tag{8.158}$$

Then, all recursively constructed functions are restricted to  $0 \leq 2t - n \leq L-1$ . Since the convergence is unique,  $x_\infty(t) = \phi(t)$  is restricted to  $[0, L-1]$  for any arbitrary  $x_0(t)$ .

The fact that the support is known can be exploited to calculate the values of  $\phi(t)$  at the times  $t_{nm} = n2^m$ . This, again, is based on the two-scale relation (8.119):

$$\phi(t) = \sqrt{2} \sum_{\ell} g_0(\ell) \phi(2t - \ell). \tag{8.159}$$

Let us assume that the initial values  $\phi(n)$  are known. By writing (8.159) as

$$\begin{aligned}\phi\left(\frac{k}{2}\right) &= \sqrt{2} \sum_{\ell} g_0(\ell) \phi(k - \ell), \\ \phi\left(\frac{k}{4}\right) &= \sqrt{2} \sum_{\ell} g_0(\ell) \phi\left(\frac{k}{2} - \ell\right), \\ &\vdots\end{aligned}\tag{8.160}$$

we realize that we obtain the intermediate values at each iteration step. However, so far we only know the values  $\phi(0) = 0$  and  $\phi(L) = 0$ . The initial values required can be determined by exploiting the fact that the initial values remain unchanged during the iteration (8.160). With

$$\mathbf{m} = [\phi(1), \dots, \phi(L-1)]^T\tag{8.161}$$

we get

$$\mathbf{m} = \mathbf{M} \cdot \mathbf{m}\tag{8.162}$$

according to (8.160), where the  $L-1 \times L-1$  matrix  $\mathbf{M}$  is given by

$$[\mathbf{M}]_{ij} := \sqrt{2} g_0(2i - j).\tag{8.163}$$

Recalling (8.140) it becomes obvious that we obtain the initial values by determining the right eigenvector  $\mathbf{m}$  of  $\mathbf{M}$  which belongs to the eigenvalue 1.

**Note.** We conclude from (8.135) and (8.138) that the sum of the even coefficients equals the sum of the odd coefficients:

$$\sum_n g_0(2n) = \sum_n g_0(2n+1) = \frac{\sqrt{2}}{2}.\tag{8.164}$$

Since the columns of  $\mathbf{M}$  contain either all even coefficients  $g_0(2n)$  or all odd coefficients  $g_0(2n+1)$ , the sum of all elements of the columns of  $\mathbf{M}$  is one. Thus, conditions (8.135) and (8.138) guarantee the existence of a left eigenvector  $[1, 1, \dots, 1]$  with eigenvalue one.

**Example.** Let  $g_0(n)$  consist of five coefficients  $g_0(0), \dots, g_0(4)$ , and let  $G_0(z)$  satisfy  $G_0(-1) = 0$ . Matrix  $\mathbf{M}$  is given by

$$\mathbf{M} = \sqrt{2} \begin{bmatrix} g_0(1) & g_0(0) & & & \\ g_0(3) & g_0(2) & g_0(1) & & \\ & g_0(4) & g_0(3) & & \end{bmatrix}.\tag{8.165}$$

Because of (8.164) we have

$$\sqrt{2} [1, 1, 1] \begin{bmatrix} g_0(1) & g_0(0) & & & \\ g_0(3) & g_0(2) & g_0(1) & & \\ & g_0(4) & g_0(3) & & \end{bmatrix} = 1 \cdot [1, 1, 1],\tag{8.166}$$

and we see that the eigenvalue 1 exists. The eigenvalue problem we have to solve is given by

$$\sqrt{2} \begin{bmatrix} g_0(1) & g_0(0) \\ g_0(3) & g_0(2) & g_0(1) \\ & g_0(4) & g_0(3) \end{bmatrix} \cdot \begin{bmatrix} \phi(1) \\ \phi(2) \\ \phi(3) \end{bmatrix} = 1 \cdot \begin{bmatrix} \phi(1) \\ \phi(2) \\ \phi(3) \end{bmatrix}. \quad (8.167)$$

## 8.7 Wavelet Families

Various wavelet families are defined in the literature. We will only consider a few of those constructed from filter banks. For further design methods the reader is referred to [36, 154].

### 8.7.1 Design of Biorthogonal Linear-Phase Wavelets

In this section, we consider the design of linear-phase biorthogonal wavelets according to Cohen, Daubechies and Feauveau [28]. We start the discussion with the first equation in (8.113), which is the PR condition for two-channel filter banks without delay. We consider an overall delay of  $\tau$ , that is

$$H_0(z)G_0(z) + H_0(-z)G_0(-z) = 2z^{-\tau}. \quad (8.168)$$

On the unit circle, this means

$$H_0(e^{j\omega})G_0(e^{j\omega}) + H_0(e^{j(\omega+\pi)})G_0(e^{j(\omega+\pi)}) = 2e^{-j\omega\tau}. \quad (8.169)$$

In order to yield linear-phase wavelets, both filter  $H_0(z)$  and  $G_0(z)$  have to be linear-phase. Furthermore, the filters need to satisfy the regularity condition as outlined in Section 8.6.6 in order to allow the construction of continuous scaling functions and wavelets.

When expressing the linear-phase property, two types of symmetry have to be considered, depending on whether the filter length is even or odd. We will outline these properties for the filter  $H_0(z)$  and start with odd-length filters. The second filter  $G_0(z)$ , which completes a perfect reconstruction pair, has the same type of symmetry.

**Odd-Length Filters.** Odd-length linear-phase filters satisfy

$$H_0(e^{j\omega}) = e^{-j\omega\tau_h} H'_0(\cos\omega), \quad (8.170)$$

where the delay  $\tau_h$  is an integer. Assuming that  $H'_0(\cos\omega)$  has  $\ell$  zeros at  $\omega = \pi$ , we may write

$$H'_0(e^{j\omega}) = \sqrt{2} \left(\cos\frac{\omega}{2}\right)^{2\ell} P(\cos\omega). \quad (8.171)$$

It is easily shown that  $G_0(e^{j\omega})$  has the same type of factorization, so that

$$G_0(e^{j\omega}) = e^{-j\omega\tau_g} \sqrt{2} \left(\cos \frac{\omega}{2}\right)^{2\tilde{\ell}} Q(\cos \omega), \quad (8.172)$$

where  $\tau = \tau_h + \tau_g$ .

**Even-Length Filters.** Symmetric even-length filters can be expressed as

$$H_0(e^{j\omega}) = e^{-j\omega(\tau_h + \frac{1}{2})} \cos \frac{\omega}{2} H'_0(\cos \omega), \quad (8.173)$$

and according to the above considerations, we may write

$$H_0(e^{j\omega}) = \sqrt{2} e^{-j\omega(\tau_h + \frac{1}{2})} \left(\cos \frac{\omega}{2}\right)^{2\ell+1} P(\cos \omega), \quad (8.174)$$

where it is again assumed that  $H_0(e^{j\omega})$  has  $\ell$  zeros at  $\omega = \pi$ .  $G_0(e^{j\omega})$  then has a factorization of the form

$$G_0(e^{j\omega}) = \sqrt{2} e^{-j\omega(\tau_g + \frac{1}{2})} \left(\cos \frac{\omega}{2}\right)^{2\tilde{\ell}+1} Q(\cos \omega). \quad (8.175)$$

**Filter Construction.** Substituting the factorizations for  $H_0(e^{j\omega})$  and  $G_0(e^{j\omega})$  into (8.169) yields

$$\left(\cos \frac{\omega}{2}\right)^{2k} M(\cos \omega) + \left(\sin \frac{\omega}{2}\right)^{2k} M(-\cos \omega) = 1 \quad (8.176)$$

with

$$M(\cos \omega) = P(\cos \omega) Q(\cos \omega) \quad (8.177)$$

and  $k = \ell + \tilde{\ell}$  if the filter length is odd and  $k = \ell + \tilde{\ell} + 1$  if it is even. This expression will now be reformulated by rewriting  $M(\cos \omega)$  as a polynomial in  $(1 - \cos \omega)/2 = \sin^2 \omega/2$ , so that  $M(\cos \omega) := F(\sin^2 \omega/2)$ . We get

$$\left(\cos \frac{\omega}{2}\right)^{2k} F(\sin^2 \omega/2) + \left(\sin \frac{\omega}{2}\right)^{2k} F(\cos^2 \omega/2) = 1, \quad (8.178)$$

or equivalently,

$$(1-x)^k F(x) + x^k F(1-x) = 1 \quad (8.179)$$

with  $x = \sin^2 \omega/2$ . Hence,

$$F(x) = (1-x)^{-k} - x^k (1-x)^{-k} F(1-x). \quad (8.180)$$

Using Bezout's theorem, one can show that this condition is satisfied by a unique polynomial  $F(x)$  with a degree of at most  $k-1$  [28]. Based on this property, the polynomial  $F(x)$  of maximum degree  $k-1$  can be found by

expanding the right-hand side of (8.180) into a Taylor series where only the first  $k$  terms are needed. This gives

$$F(x) = \sum_{n=0}^{k-1} \binom{k+n-1}{n} x^n. \quad (8.181)$$

The general solution of higher degree can be written as

$$F(x) = \sum_{n=0}^{k-1} \binom{k+n-1}{n} x^n + x^k R(1-2x), \quad (8.182)$$

where  $R(x)$  is an odd polynomial. Based on this expression, filters can be found by factorizing a given  $F(\sin^2 \omega/2)$  into  $P(\cos \omega)$  and  $Q(\cos \omega)$ . Given  $P(\cos \omega)$  and  $Q(\cos \omega)$  one easily finds  $H_0(e^{j\omega})$  and  $G_0(e^{j\omega})$  from (8.170) – (8.175).

**Spline Wavelets.** Spline wavelets based on odd-length filters are constructed by choosing  $R(x) \equiv 0$  and

$$G_0(e^{j\omega}) = \sqrt{2} e^{-j\omega\tau_g} \left( \cos \frac{\omega}{2} \right)^{2\tilde{\ell}}. \quad (8.183)$$

The corresponding analysis filter is

$$H_0(e^{j\omega}) = \sqrt{2} e^{-j\omega\tau_h} \left( \cos \frac{\omega}{2} \right)^{2\ell} \sum_{n=0}^{\ell+\tilde{\ell}-1} \binom{\ell+\tilde{\ell}+n-1}{n} \left( \sin^2 \frac{\omega}{2} \right)^n. \quad (8.184)$$

Even-length filters are given by

$$G_0(e^{j\omega}) = \sqrt{2} e^{-j\omega(\tau_g + \frac{1}{2})} \left( \cos \frac{\omega}{2} \right)^{2\tilde{\ell}+1} \quad (8.185)$$

and

$$H_0(e^{j\omega}) = \sqrt{2} e^{-j\omega(\tau_h + \frac{1}{2})} \left( \cos \frac{\omega}{2} \right)^{2\ell+1} \sum_{n=0}^{\ell+\tilde{\ell}} \binom{\ell+\tilde{\ell}+n}{n} \left( \sin^2 \frac{\omega}{2} \right)^n. \quad (8.186)$$

The scaling function  $\phi(t)$  constructed from  $G_0(z)$  according to (8.183) is a B-spline centered around  $\tau_g$ , and the one constructed from  $G_0(z)$  according to (8.185) is a B-spline centered around  $\tau_g + \frac{1}{2}$ .

**Filters with Almost Equal Length.** In the spline case, the length of  $H_0(z)$  is typically much higher than the length of  $G_0(z)$ . In order to design filters with almost equal length, one groups the zeros of  $F(x)$  into real zeros and pairs of conjugate complex zeros and rewrites  $F(x)$  as

$$F(x) = A \prod_{i=1}^I (x - x_i) \prod_{j=1}^J (x^2 - 2\Re\{z_j\}x + |z_j|). \tag{8.187}$$

Any regrouping into two polynomials yields a PR filter pair. This allows us to choose filters with equal or almost equal length. For example, the 9-7 filters have been found this way [28]; they are known for their excellent coding performance in wavelet-based image compression [155, 134].

**Examples.** Table 8.1 shows some examples of odd-length filters. While the coefficients of the spline filters (5-3 and 9-3) are dyadic fractions, those of the 9-7 filters constructed from (8.187) are not even rational. This means an implementation advantage for the spline filters in real-time applications. However, the 9-7 filters have superior coding performance. For illustration, Figures 8.15 and 8.16 show the analysis and synthesis scaling functions and wavelets generated from the 9-3 and 9-7 filters in Table 8.1.

**Table 8.1.**  
Linear-phase odd-length biorthogonal wavelet filters.

| $n$ | 5-3           |               | 9-3            |                | 9-7               |                   |
|-----|---------------|---------------|----------------|----------------|-------------------|-------------------|
|     | $4 \cdot g_0$ | $4 \cdot h_0$ | $16 \cdot g_0$ | $16 \cdot h_0$ | $g_0$             | $h_0$             |
| 0   | 1             | -1            | 1              | 3              | -0.06453888265083 | 0.03782845543778  |
| 1   | 2             | 2             | 2              | -6             | -0.04068941758680 | -0.02384946495431 |
| 2   | 1             | 6             | 1              | -16            | 0.41809227351029  | -0.11062440401143 |
| 3   |               | 2             |                | 38             | 0.78848561689252  | 0.37740285554759  |
| 4   |               | -1            |                | 90             | 0.41809227351029  | 0.85269867833384  |
| 5   |               |               |                | 38             | -0.04068941758680 | 0.37740285554759  |
| 6   |               |               |                | -16            | -0.06453888265083 | -0.11062440401143 |
| 7   |               |               |                | -6             |                   | -0.02384946495431 |
| 8   |               |               |                | 3              |                   | 0.03782845543778  |

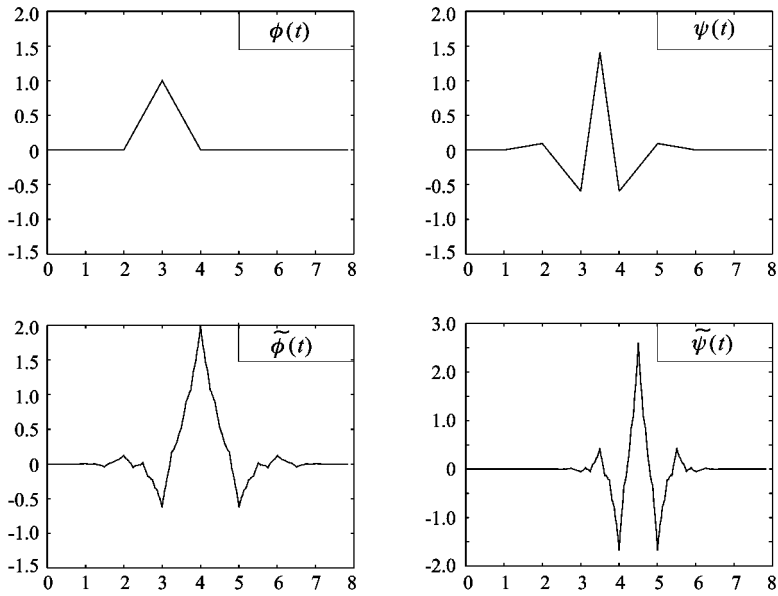


Figure 8.15. Scaling functions and wavelets constructed from the 9-3 filters.

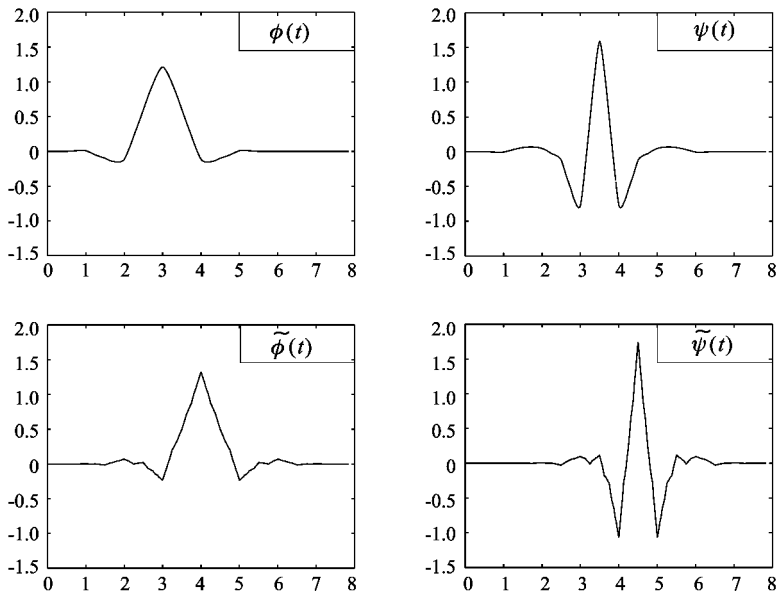


Figure 8.16. Scaling functions and wavelets constructed from the 9-7 filters.

### 8.7.2 The Orthonormal Daubechies Wavelets

Daubechies designed a family of orthonormal wavelets with a maximal number of vanishing moments for a given support [34]. In order to control the regularity, the following factorization of  $H_0(e^{j\omega})$  is considered:

$$H_0(e^{j\omega}) = \sqrt{2} \left( \frac{1 + e^{-j\omega}}{2} \right)^k P(e^{j\omega}). \quad (8.188)$$

Because of orthonormality, the PR condition to be met by the prototype filter is

$$\left| H_0(e^{j\omega}) \right|^2 + \left| H_0(e^{j(\omega + \pi)}) \right|^2 = 2. \quad (8.189)$$

Since  $h_0(n)$  is considered to be real, the term  $|H_0(e^{j\omega})|^2$  may be written as

$$\left| H_0(e^{j\omega}) \right|^2 = \sqrt{2} \left( \cos^2 \frac{\omega}{2} \right)^k M(\cos \omega) \quad (8.190)$$

with

$$M(\cos \omega) = |P(e^{j\omega})|^2. \quad (8.191)$$

Inserting (8.190) into (8.189) yields

$$\left( \cos^2 \frac{\omega}{2} \right)^k M(\cos \omega) + \left( \sin^2 \frac{\omega}{2} \right)^k M(-\cos \omega) = 1. \quad (8.192)$$

Using the same arguments as in the last section, (8.192) can also be written as

$$\left( \cos^2 \frac{\omega}{2} \right)^k F(\sin^2 \omega/2) + \left( \sin^2 \frac{\omega}{2} \right)^k F(\cos^2 \omega/2) = 1, \quad (8.193)$$

or equivalently as

$$(1-x)^k F(x) + x^k F(1-x) = 1 \quad (8.194)$$

with  $x = \sin^2 \omega/2$ . This is essentially the same condition that occurred in the biorthogonal case, but we now have to satisfy  $F(\sin^2 \omega/2) \geq 0 \forall \omega$ , because  $F(\sin^2 \omega/2) = |P(e^{j\omega})|^2$ .

Daubechies proposed to choose

$$F(x) = \sum_{n=0}^{k-1} \binom{k+n-1}{n} x^n + x^k R(1-2x), \quad (8.195)$$

where  $R(x)$  is an odd polynomial such that  $F(x) \geq 0$  for  $x \in [0, 1]$ . The family of Daubechies wavelets is derived for  $R(x) \equiv 0$  by spectral factorization of  $F(x)$  into  $F(x) = P(x)P(x^{-1})$ . For this, the zeros of  $F(x)$  have to be computed and grouped into zeros inside and outside the unit circle.  $P(x)$  then

contains all zeros inside the unit circle. This factorization results in minimum phase scaling functions. For filters  $H_0(z)$  with at least eight coefficients, more symmetric factorizations are also possible. The magnitude frequency responses, however, are the same as for the minimum phase case.

Figure 8.17 shows some Daubechies wavelets, the corresponding scaling functions and the frequency responses of the filters. We observe that the scaling functions and wavelets become smoother with increasing filter length. For comparison, some Daubechies wavelets with maximal symmetry, known as *symmlets*, and the corresponding scaling functions are depicted in Figure 8.18. The frequency responses are the same as in Figure 8.17. Recall that with a few exceptions (Haar and Shannon wavelets), perfect symmetry is impossible.

### 8.7.3 Coiflets

The orthonormal Daubechies wavelets have a maximum number of vanishing wavelet moments for a given support. Vanishing moments of the scaling function have not been considered. The idea behind the Coiflet wavelets is to trade off some of the vanishing wavelet moments to the scaling function. This can be expressed as

$$\int_{-\infty}^{\infty} t^k \phi(t) dt = \begin{cases} 1, & \text{for } k = 0 \\ 0, & \text{for } k = 1, 2, \dots, \ell - 1 \end{cases} \quad (8.196)$$

and

$$\int_{-\infty}^{\infty} t^k \psi(t) dt = 0 \quad \text{for } k = 0, 1, \dots, \ell - 1. \quad (8.197)$$

Note that the 0th moments of a scaling function is still fixed to one. Further note that the same parameter  $\ell$ , called the order of the coiflet, is used for the wavelet and the scaling function.

The frequency domain formulations of (8.196) and (8.197) are

$$\left. \frac{d^k \omega \Phi(\omega)}{d\omega^k} \right|_{\omega=0} = \begin{cases} 1, & \text{for } k = 0 \\ 0, & \text{for } k = 1, 2, \dots, \ell - 1 \end{cases} \quad (8.198)$$

and

$$\left. \frac{d^k \omega \Psi(\omega)}{d\omega^k} \right|_{\omega=0} = 0 \quad \text{for } k = 0, 1, \dots, \ell - 1. \quad (8.199)$$

Condition (8.198) means for the filter  $H_0(e^{j\omega})$  that

$$H_0(e^{j\omega}) = 1 + (1 - e^{-j\omega})^\ell U(e^{j\omega}) \quad (8.200)$$

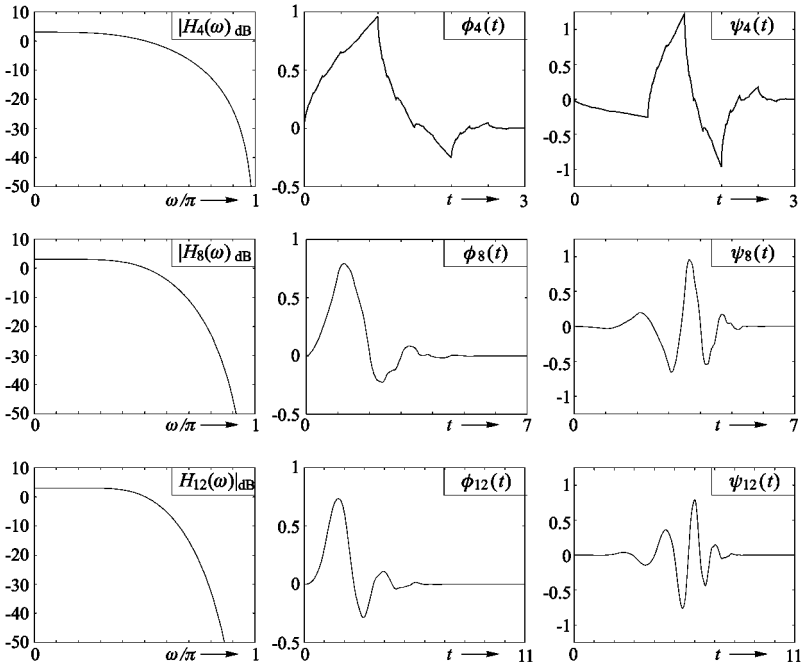


Figure 8.17. Frequency responses of the minimum-phase Daubechies filters and the corresponding scaling functions and wavelets (the indices indicate filter length).

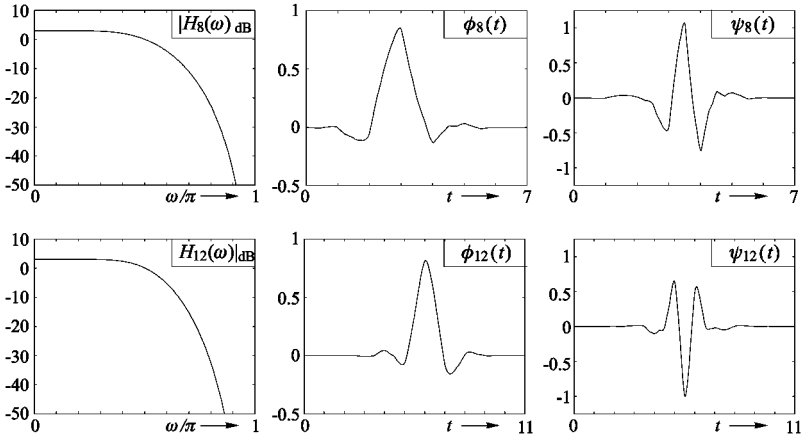


Figure 8.18. Frequency responses of the maximally symmetric Daubechies filters and the corresponding scaling functions and wavelets (the indices indicate filter length; the frequency responses are equal to those in Figure 8.17).

for some  $U(e^{j\omega})$ . From (8.199) it follows that  $H_0(e^{j\omega})$  can also be written in the form (8.188)

$$H_0(e^{j\omega}) = \sqrt{2} \left( \frac{1 + e^{-j\omega}}{2} \right)^\ell P(e^{j\omega}). \quad (8.201)$$

For even  $\ell$ , solutions to this problem can be formulated as [36]

$$P(e^{j\omega}) = \sum_{n=0}^{\ell/2-1} \binom{\ell/2 + n - 1}{n} \left( \sin^2 \frac{\omega}{2} \right)^n + \left( \sin^2 \frac{\omega}{2} \right)^{\frac{\ell}{2}} f(e^{j\omega}), \quad (8.202)$$

where  $f(e^{j\omega})$  has to be found such that (8.189) is satisfied. This results in  $\ell/2$  quadratic equations for  $\ell/2$  unknowns [36].

## 8.8 The Wavelet Transform of Discrete-Time Signals

In the previous sections we assumed continuous-time signals and wavelets throughout. It could be shown that sample values of the wavelet transform can be computed by means of a PR filter bank, provided the coefficients  $c_0(n)$  for representing an approximation  $x_0(t) = \sum_n c_0(n) \tilde{\phi}(t - n)$  are known. For the sequences  $d_m(n)$ ,  $m > 0$ , successively computed from  $c_0(n)$ , we had

$$\begin{aligned} d_m(n) &= \mathcal{W}_x(2^m n, 2^m) = \langle x, \psi_{mn} \rangle \\ &= 2^{-\frac{m}{2}} \int_{-\infty}^{\infty} x(t) \psi^*(2^{-m}t - n) dt, \end{aligned} \quad (8.203)$$

that is, the values  $d_m(n)$  were sample values of the wavelet transform of a continuous-time signal. A considerable problem is the generation of the discrete-time signal  $c_0(n)$  because in digital signal processing the signals to be processed are usually obtained by filtering continuous-time signals with a standard anti-aliasing filter and sampling. Only if the impulse response  $h(t)$  of the prefilter is chosen such that  $x_0(t) = x(t) * h(t) \in V_0$ , we obtain a “genuine” wavelet analysis.

If we wish to apply the theory outlined above to “ordinary” discrete-time signals  $x(n)$ , it is helpful to discretize the integral in (8.203):

$$w_x(2^m n, 2^m) = 2^{-\frac{m}{2}} \sum_k x(k) \psi^*(2^{-m}k - n). \quad (8.204)$$

Here, the values  $\psi(2^{-m}k - n)$ ,  $m > 0$ ,  $k, n \in \mathbb{Z}$  are to be regarded as samples of a given wavelet  $\psi(t)$  where the sampling interval is  $T = 1$ .

**Translation Invariance.** We are mainly interested in dyadically arranged values according to (8.204). In this form the wavelet analysis is not translation invariant because a delayed input signal  $x(n - \ell)$  leads to

$$\begin{aligned} w_x(2^m(n - 2^{-m}\ell), 2^m) &= 2^{-\frac{m}{2}} \sum_k x(k - \ell) \psi^*(2^{-m}k - n) \\ &= 2^{-\frac{m}{2}} \sum_i x(i) \psi^*(2^{-m}i - [n - 2^{-m}\ell]). \end{aligned} \quad (8.205)$$

Only if  $\ell$  is a multiple of  $2^m$ , we obtain shifted versions of the same wavelet coefficients. However, for many applications such as pattern recognition or motion estimation in the wavelet domain it is desirable to achieve translation invariance. This problem can be solved by computing all values

$$w_x(n, 2^m) = 2^{-\frac{m}{2}} \sum_k x(k) \psi^*(2^{-m}(k - n)). \quad (8.206)$$

In general, this is computationally very expensive, but when using the à trous algorithm outlined in the next section, the computation is as efficient as with the DWT.

### 8.8.1 The À Trous Algorithm

A direct evaluation of (8.204) and (8.206) is very costly if the values of the wavelet transform must be determined for several octaves because the number of filter coefficients roughly doubles from octave to octave. Here, the so-called *à trous algorithm* allows efficient evaluation with respect to computing effort. This algorithm has been proposed by Holschneider *et al.* [73] and Dutilleul [48]. The relationship between the à trous and the Mallat algorithm was derived by Shensa [132].

We start with dyadic sampling according to (8.204). The impulse response of the filter  $H_1(z)$  is chosen to be

$$h_1(n) = 2^{-\frac{1}{2}} \psi^*(-n/2). \quad (8.207)$$

With this filter the output values of the first stage of the filter bank in Figure 8.19 are equal to those according to (8.204), we have

$$w_x(2n, 2) = \tilde{w}_x(2n, 2).$$

The basic idea of the à trous algorithm is to evaluate equation (8.204) not exactly, but approximately. For this, we use an interpolation filter as

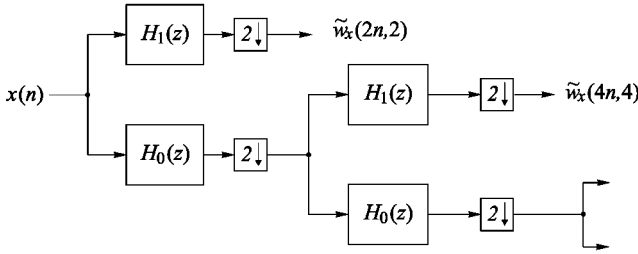


Figure 8.19. Analysis filter bank.

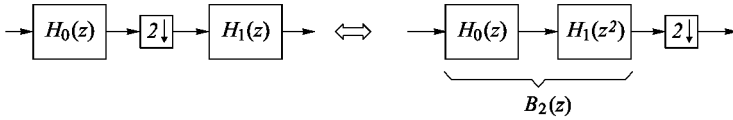


Figure 8.20. Equivalent arrangements.

the analysis lowpass  $H_0(z)$ .<sup>4</sup> This may for instance be a Lagrange halfband filter, but in principle any interpolation filter will do. In order to explain this approach in more detail let us take a look at the flow graphs shown in Figure 8.20, which both have the transfer function  $\frac{1}{2} H_1(z^2) [H_0(z) + H_0(-z)]$ . The transfer function  $B_2(z)$  is

$$B_2(z) = H_0(z) H_1(z^2). \tag{8.208}$$

If  $H_0(z)$  is an interpolation filter, (8.208) can be interpreted as follows: first we insert zeros into the impulse response  $h_1(n)$ . By convolving the upsampled impulse response  $h'_1(2n) = h_1(n)$ ,  $h'_1(2n + 1) = 0$  with the interpolation filter the values  $h'_1(2n)$  remain unchanged, while the values  $h'_1(2n + 1)$  are interpolated. Thus, the even numbered values of the impulse response  $b_2(n) \longleftrightarrow B_2(z)$  are equal to the even numbered samples of  $2^{-1}\psi^*(-n/4)$ . The interpolated intermediate values are approximately the sample values of  $2^{-1}\psi^*(-n/4)$  at the odd positions. Thus, we have

$$b_2(n) \approx 2^{-1} \psi^*(-n/4). \tag{8.209}$$

Iteration of this approach yields

$$B_m(z) = \begin{cases} H_1(z), & \text{for } m = 1, \\ H_1(z^{2^{m-1}}) \prod_{j=0}^{m-2} H_0(z^{2^j}), & \text{for } m > 1. \end{cases} \tag{8.210}$$

<sup>4</sup>The term “à trous” means “with gaps”, which refers to the fact that an interpolation lowpass filter is used.

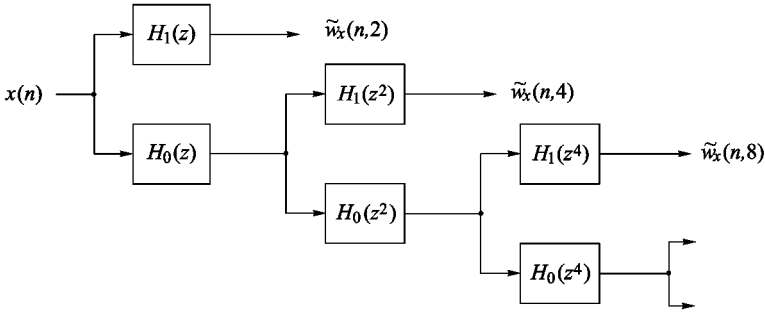


**Figure 8.21.** Filter bank for computing wavelet coefficients.

For the impulse responses  $b_m(n) \longleftrightarrow B_m(z)$  we get

$$b_m(n) \approx 2^{-\frac{m}{2}} \psi^*(-2^{-m}n), \quad m \geq 1. \tag{8.211}$$

The values  $\tilde{w}_x(2^m n, 2^m)$  computed with the filter bank in Figure 8.19 are given by

$$\tilde{w}_x(2^m n, 2^m) \approx w_x(2^m n, 2^m). \tag{8.212}$$

Thus, the scheme in Figure 8.19 yields an approximate wavelet analysis.

**Oversampled Wavelet Series.** Although the coefficients of critically sampled representations contain all information on the analyzed signal, they suffer from the drawback that the analysis is not translation invariant. The aim is now to compute an approximation of

$$w_x(n, 2^m) = 2^{-\frac{m}{2}} \sum_k x(k) \psi^*(2^{-m}(k - n)) \tag{8.213}$$

by means of the filters  $b_m(n) \longleftrightarrow B_m(z)$  according to (8.210):

$$\tilde{w}_x(n, 2^m) = 2^{-\frac{m}{2}} \sum_k x(k) b_m(n - k) \tag{8.214}$$

While the direct evaluation of these formulae means high computational cost, the values  $\tilde{w}_x(n, 2^m)$  may be efficiently computed by use of the filter bank in Figure 8.21. The filters  $H_0(z^{2^m})$  and  $H_1(z^{2^m})$ ,  $m > 1$ , can be realized in polyphase structure. The number of operations that have to be carried out is very small so that such an evaluation is suitable for real-time applications also.

In many cases the frequency resolution of a pure octave-band analysis is not sufficient. An improved resolution can be obtained by implementing  $M$

octave filter banks in parallel where each bank covers only an  $M$ th part of the octaves. This concept has been discussed in Section 8.4.2 for the continuous-time case. The application to a discrete-time analysis based on the à trous algorithm is straightforward.

### 8.8.2 The Relationship between the Mallat and À Trous Algorithms

The discussion above has shown that the only formal difference between the filters used in the Mallat and à trous algorithms lies in the fact that in the Mallat algorithm the impulse response of the filter  $H_1(z)$  does not, in general, consist of sample values of the continuous-time wavelet. However, both concepts can easily be reconciled. For this, let us consider a PR two-channel filter bank, where  $H_0(z)$  is an interpolation filter and where  $H_1(z)$  satisfies  $H_1(1) = 0$ . Based on the filter bank we can construct the associated continuous-time scaling functions and wavelets. Since  $H_0(z)$  is supposed to be an interpolation filter, we have the following correspondence between the impulse response of the highpass filter,  $h_1(n)$ , and the sample values of the wavelet  $\psi(t)$ , which is iteratively determined from  $h_0(n)$  and  $h_1(n)$ :

$$h_1(n) = 2^{-\frac{1}{2}} \psi^*(-n/2). \quad (8.215)$$

For the filters  $B_m(z)$  defined in (8.210) we have

$$b_m(n) = 2^{-\frac{m}{2}} \psi^*(-2^{-m}n), \quad (8.216)$$

and we derive

$$\tilde{w}_x(2^m n, 2^m) = w_x(2^m n, 2^m). \quad (8.217)$$

This means that the à trous algorithm computes the wavelet transform exactly if  $H_0(z)$  and  $H_1(z)$  belong to a PR two-channel filter bank while  $H_0(z)$  is an interpolation filter. Then, all computed wavelet coefficients  $w_x(2^m n, 2^m)$ ,  $m > 0$ , can be interpreted as sample values of a continuous wavelet transform provided the demand for regularity is met:  $w_x(2^m n, 2^m) = \mathcal{W}_x(2^m n, 2^m)$ ,  $m > 0$ .

In order to determine filters that yield perfect wavelet analyses of discrete-time signals with  $\tilde{w}_x(2^m k, 2^m) = w_x(2^m n, 2^m)$  we may proceed as follows: we take an interpolation filter  $H_0(z)$  and compute a filter  $G_0(z)$  such that

$$\sum_n g_0(n) h_0(2\ell - n) = \delta_{\ell 0}. \quad (8.218)$$

Note that (8.218) is just an underdetermined linear set of equations. From  $H_0(z)$  and  $G_0(z)$  we can then calculate the filters  $H_1(z)$  and  $G_1(z)$  according to equation (6.22) and can construct the wavelet via iteration. The solution to (8.218) is not unique, so that one can choose a wavelet which has the desired properties.

**Example.** For the analysis lowpass we use a binary filter with 31 coefficients as given in (8.181). The length of the analysis highpass is restricted to 63 coefficients. The overall delay of the analysis-synthesis system is chosen such that a linear-phase highpass is yielded. Figures 8.22(a) and 8.22(b) show the respective scaling function, the wavelet, and the sample values  $\phi(-n/2) = h_0(n)$  and  $\psi(-n/2) = h_1(n)$ . The frequency responses of  $H_0(z)$  and  $H_1(z)$  are pictured in Figure 8.22(c).

### 8.8.3 The Discrete-Time Morlet Wavelet

The Morlet wavelet was introduced in Section 8.2. In order to realize a wavelet analysis of discrete-time signals, the wavelet is sampled in such a way that

$$h_1(n) = b_1(n) = e^{j\omega_0 n} e^{-\beta^2 n^2/2}, \quad (8.219)$$

where  $b_1(n)$  is defined as in (8.210). In order to obtain a “practically” admissible and analytic wavelet we choose

$$2\pi\beta \leq \omega_0 \leq \pi/2. \quad (8.220)$$

In the discrete-time case a further problem arises due to the periodicity of the spectra. In order to ensure that we achieve an analytic wavelet we have to demand that

$$\Psi(e^{j\omega}) = 0 \quad \text{for} \quad \pi < \omega \leq 2\pi.$$

In order to guarantee this, at least approximately, the parameters  $\omega_0$  and  $\beta$  are chosen such that

$$\omega_0 \leq \pi - \sqrt{2} \beta \quad (8.221)$$

is also satisfied [132].

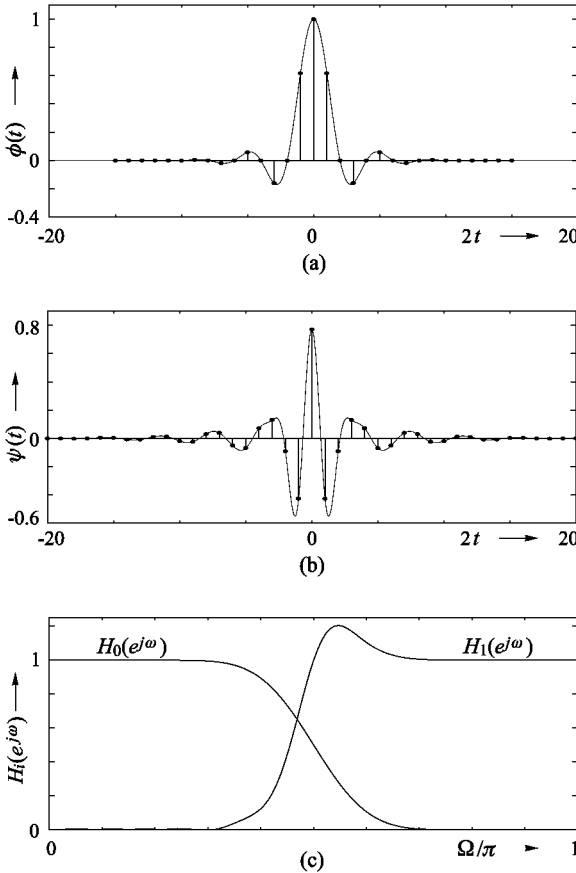


**Figure 8.22.** Example; (a) scaling function  $\phi(t)$  and the sample values  $\phi(-nT/2) = h_0(n)$ ; (b) wavelet  $\psi(t)$  and the sample values  $\psi(-nT/2) = h_1(n)$ ; (c) frequency responses of the analysis filters.

## 8.9 DWT-Based Image Compression

Image compression based on the DWT is essentially equivalent to compression based on octave-band filter banks as outlined in Section 6.8. The strategy is as follows: the image is first decomposed into a set of subband signals by using a separable<sup>5</sup> 2-D filter bank. Then, the subband samples are quantized and further compressed. The filters, however, satisfy certain conditions such as regularity and vanishing moments.

To give an example of the discrete wavelet transform of a 2-D signal,

<sup>5</sup>Non-separable 2-D wavelets and filter banks are not considered throughout this book.

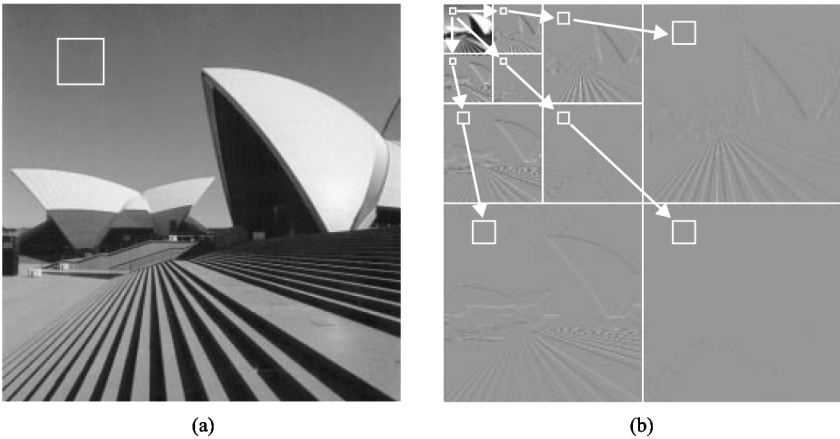


**Figure 8.23.** Separable 2-D discrete wavelet transform; (a) original; (b) DWT.

Figure 8.23(a) shows an original image and Figure 8.23(b) shows its 2-D wavelet transform. The squares in Figure 8.23(b) indicate spatial regions that belong to the same region in Figure 8.23(a). The arrows indicate parent-child relationships. An important observation can be made from Figure 8.23(b), which is true for most natural images: if there is little low-frequency information in a spatial region, then it is likely that there is also little high-frequency information in that region. Thus, if a parent pixel is small, then it is likely that the belonging children are also small. This relationship can be exploited in order to encode the subband pixels in an efficient way. The coding technique is known as *embedded zerotree wavelet coding* [131, 128].

We will not study the embedded zerotree coding here in great detail, but we will give a rough idea of how such a coder works. Most importantly, the quantization of the wavelet coefficients is carried out successively, using a bitplane technique. One starts with a coarse quantization and refines it in every subsequent step. Whenever a tree of zeros (pixels quantized to zero with respect to a given threshold) is identified, it will be coded as a so-called zerotree by using a single codeword. Starting with coarse quantization ensures that a high number of zerotrees can be identified at the beginning of the encoding process. During the refinement process, when the quantization step size is successively reduced, the number of zerotrees successively decreases. Overall one gets an embedded bitstream where the most important information (in terms of signal energy) is coded first. The refinement process can be continued until one reaches a desired precision. One of the most interesting features of this coding technique is that the bitstream can be truncated at any position, resulting in an almost optimal rate-distortion behavior for any bit rate.

## 8.10 Wavelet-Based Denoising

The aim of denoising is to remove the noise  $w(n)$  from a signal

$$y(n) = x(n) + w(n). \quad (8.222)$$

For example,  $w(n)$  may be a Gaussian white noise process, which is statistically independent of  $x(n)$ . One tries to remove the noise by applying a non-linear operation to the wavelet representation of  $y(n)$ . The same problem has been addressed in Chapter 7.3 in the context of the STFT, where it was solved via spectral subtraction. In fact, wavelet-based denoising is closely related to spectral subtraction. The main difference between both approaches lies in the fact that the wavelets used for denoising are real-valued while the STFT is complex.

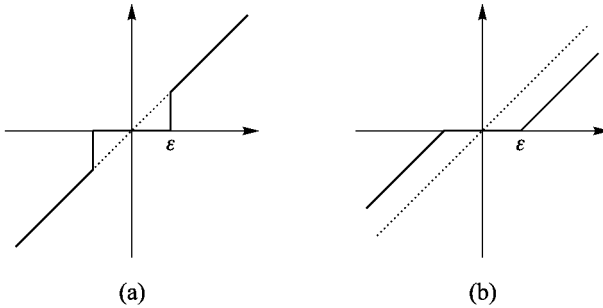


**Figure 8.24.** Thresholding techniques; (a) hard; (b) soft thresholding.

The denoising procedure is as follows. First, the signal  $y(n)$  is decomposed using an octave-band filter bank, thus performing a discrete wavelet transform. Then, the wavelet coefficients are manipulated in order to remove the noise component. Two approaches known as *hard* and *soft thresholding* have been proposed for this purpose [43, 42]. They use the following non-linearities:

$$\hat{y}(n) = \begin{cases} y(n), & y(n) > \varepsilon \\ y(n), & y(n) < -\varepsilon \\ 0, & |y(n)| \leq \varepsilon \end{cases} \quad (\text{hard}) \quad (8.223)$$

$$\hat{y}(n) = \begin{cases} y(n) - \varepsilon, & y(n) > \varepsilon \\ y(n) + \varepsilon, & y(n) < -\varepsilon \\ 0, & |y(n)| \leq \varepsilon \end{cases} \quad (\text{soft}) \quad (8.224)$$

Figure 8.24 illustrates both techniques.

Basically, the idea of thresholding is that  $x(n)$  can be represented via a few wavelet coefficients, while the noise has wideband characteristics and spreads out on all coefficients. For example, this holds true if  $x(n)$  is a lowpass signal, while  $w(n)$  is white noise. The thresholding procedure then sets the small wavelet coefficients representing  $w(n)$  to zero, while the large coefficients due to  $x(n)$  are only slightly affected. Thus, provided the threshold  $\varepsilon$  is chosen appropriately, the signal  $\hat{y}(n)$  reconstructed from the manipulated wavelet coefficients will contain much less noise than  $y(n)$  does. In practice, the problem is to choose  $\varepsilon$ , because the amount of noise is usually not known *a priori*. If  $\varepsilon$  is too small, the noise will not be efficiently removed. If it is too large, the signal will be distorted.